A&A 560, A11 (2013)
DOI: 10.1051/0004-6361/201321412

Astronomy & Astrophysics

The circumstellar environment and evolutionary state of the supergiant B[e] star Wd1-9⋆,⋆⋆

J. S. Clark[1], B. W. Ritchie[1], and I. Negueruela[2]

[1] Department of Physics and Astronomy, The Open University, Walton Hall, Milton Keynes MK7 6AA, UK
e-mail: s.clark@open.ac.uk
[2] Departamento de Física, Ingeniería de Sistemas y Teoría de la Señal, Universidad de Alicante, Apdo. 99, 03080 Alicante, Spain

Received 5 March 2013 / Accepted 3 October 2013

ABSTRACT

Context. Historically, supergiant (sg)B[e] stars have been difficult to include in theoretical schemes for the evolution of massive OB stars.
Aims. The location of Wd1-9 within the coeval starburst cluster Westerlund 1 means that it may be placed into a proper evolutionary context and we therefore aim to utilise a comprehensive multiwavelength dataset to determine its physical properties and consequently its relation to other sgB[e] stars and the global population of massive evolved stars within Wd1.
Methods. Multi-epoch *R*- and *I*-band VLT/UVES and VLT/FORS2 spectra are used to constrain the properties of the circumstellar gas, while an ISO-SWS spectrum covering 2.45–45 μm is used to investigate the distribution, geometry and composition of the dust via a semi-analytic irradiated disk model. Radio emission enables a long term mass-loss history to be determined, while X-ray observations reveal the physical nature of high energy processes within the system.
Results. Wd1-9 exhibits the rich optical emission line spectrum that is characteristic of sgB[e] stars. Likewise its mid-IR spectrum resembles those of the LMC sgB[e] stars R66 and 126, revealing the presence of equatorially concentrated silicate dust, with a mass of $\sim 10^{-4} M_{\odot}$. Extreme historical and ongoing mass loss ($\gtrsim 10^{-4}$ $M_{\odot}$ yr^{-1}) is inferred from the radio observations. The X-ray properties of Wd1-9 imply the presence of high temperature plasma within the system and are directly comparable to a number of confirmed short-period colliding wind binaries within Wd1.
Conclusions. The most complete explanation for the observational properties of Wd1-9 is that it is a massive interacting binary currently undergoing, or recently exited from, rapid Roche-lobe overflow, supporting the hypothesis that binarity mediates the formation of (a subset of) sgB[e] stars. The mass loss rate of Wd1-9 is consistent with such an assertion, while viable progenitor and descendent systems are present within Wd1 and comparable sgB[e] binaries have been identified in the Galaxy. Moreover, the rarity of sgB[e] stars – only two examples are identified from a census of ∼68 young massive Galactic clusters and associations containing ∼600 post-Main Sequence stars – is explicable given the rapidity ($\sim 10^4$ yr) expected for this phase of massive binary evolution.

Key words. binaries: close – circumstellar matter – stars: emission-line, Be

1. Introduction

Supergiant (sg)B[e] stars are luminous, evolved objects that display the B[e] phenomenon – strong Balmer-series emission lines, permitted emission lines from low-ionization metals and forbidden lines of [Fe II] and [O I] in the optical spectrum and a strong infra-red excess from hot dust (Lamers et al. 1998). These features are thought to originate in a non-spherical geometry in which the gaseous and dusty circumstellar material is concentrated in equatorial regions, while broad UV resonance absorption lines indicate a fast, low-density polar wind (Zickgraf et al. 1985). Notwithstanding these uniform classification criteria, pronounced differences in both spectral morphologies (e.g. Zickgraf et al. 2003) and the quantity and temperature of circumstellar dust (cf. Kastner et al. 2006, 2010; Graus et al. 2012) are present in sgB[e] stars, which also span an unexpectedly wide range of intrinsic luminosities ($\log(L_{\rm bol}/L_{\odot}) \sim 4$–6; Gummersbach et al. 1995).

The physical mechanism(s) driving the mass loss that sculpts the complex circumstellar environments of sgB[e] stars is unclear at present (Hillier et al. 2006) and its elucidation is hampered by the intrinsic rarity of such stars (Sect. 6.1.2). Luminous blue variables (LBVs) and sgB[e] stars are co-located in the Hertzsprung-Russell diagram and display spectroscopic similarities, leading to suggestions of an evolutionary link (e.g. Stothers & Chin 1996), while the bluewards evolution and current asymmetric wind of the peculiar cool hypergiant IRC +10 420 implies a possible relationship between B[e] supergiants and post-red supergiants (RSG; Davies et al. 2007b). More recently, much interest has focused on the role of binarity in triggering the B[e] phenomenon, either via merger (e.g. Podsiadlowski et al. 2006) or binary driven mass loss (e.g. Zickgraf et al. 2003, Kastner et al. 2006); we return to this hypothesis in more detail in Sect. 6.

In this paper we examine the multiwavelength properties of the sgB[e] star Wd1-9 (=*Ara C* in the notation of Borgman et al. 1970), in the starburst cluster Westerlund 1 (hereafter Wd1; Westerlund 1961). Classified as a Be star by Westerlund (1987) and a sgB[e] star by Clark et al. (2005), Wd1-9 is radio, mid-IR and X-ray bright (Clark et al. 1998, 2008; Dougherty et al. 2010) and displays a rich emission line spectrum with a complete absence of any photospheric absorption features. The evolved state of Wd1-9 is firmly established by its membership

⋆ This work is based on observations collected at the European Southern Observatory, Paranal (programme IDs ESO 087.D-0355, 087.D-0440, 087.D-0673, and 073.D-0327) and uses the ISO-SWS database of Sloan et al. (2003).
⋆⋆ Table 1 and Appendix A are available in electronic form at http://www.aanda.org

of Wd1, which hosts a unique coeval population of massive, post-main sequence (MS) stars that include Wolf-Rayets (WRs), numerous OB supergiants, four RSGs and a population of ten B5–F8 hypergiants with initial masses ~35−40 $M_{\odot}$ (Ritchie et al. 2010a; Negueruela et al. 2010a). In this regard the radio observations of Wd1-9 are of particular interest, indicating a recent phase of enhanced or eruptive mass loss, characteristic of either an LBV or interacting binary nature (Dougherty et al. 2010, Sect. 6).

The structure of the paper is as follows. In Sect. 2 we briefly describe our observations and data reduction, while in Sect. 3 we describe the optical spectrum in detail. Section 4 describes the IR properties of Wd1-9. In Sect. 5 we discuss Wd1-9 in the context of other sgB[e] stars and in Sect. 6 we consider its evolutionary state before summarising our findings in Sect. 7.

2. Observations and data reduction

Wd1-9 was subject to an intensive VLT observing programme during 2011 April, with dates and instrument configurations listed in Table 1. High resolution *R*- and *I*-band spectra were obtained in service mode on three nights using the Ultraviolet and Visual Echelle Spectrograph (UVES; Dekker et al. 2000) located on VLT UT2 *Kueyen* at Cerro Paranal, Chile. On the first two nights (April 6 and 14) UVES was used with the red arm, cross-disperser CD#4 and a central wavelength of 8600 Å, while on the third night (April 25) dichoric 2 mode was used, with the red arm using cross-disperser CD#4 and a central wavelength of 7600 Å. On all three nights image slicer #1 was used, giving a resolving power $R \sim 60\,000$, with the combination of red and dichoric modes providing continual spectral coverage from below 6000 Å to 10 420 Å. Spectra were reduced using the UVES pipeline[1], version 4.9.5 and the Common Pipeline Library, version 5.3.1, while final extraction, correction for heliocentric motion and data analysis were carried out using the IRAF[2] *onedspec* tasks.

In order to search for longer-term evolutionary trends in the spectrum of Wd1-9, we made use of additional intermediate resolution spectra obtained with the Fibre Large Array Multi Element Spectrograph (FLAMES; Pasquini et al. 2002), again located on VLT UT2 *Kueyen*, and the spectro-imager FORS2 (Appenzeller et al. 1998), located on VLT UT1 *Antu*. FLAMES spectra were obtained on 2011 April 17, May 22 and June 24 using the HR21 setup, which provides coverage from 8484–9001 Å with $R \sim 16\,200$; data reduction is as described in Ritchie et al. (2009a). Six FORS2 spectra acquired on 2011 April 16 and 2004 June 12–14 were also utilised. On all occasions FORS2 was used in longslit mode (0.″3 slit) with grisms G1200R (5750–7310 Å) and G1028z (7730–9480 Å), giving $R \sim 7000$; the FORS2 configuration and data reduction is described in Negueruela et al. (2010a). While these data are of lower resolution than the main UVES dataset, the FLAMES spectra allow examination of strong hydrogen, calcium and nitrogen lines in the months after the UVES observations, while the FORS2 spectra use identical configurations and therefore provide a seven-year baseline unaffected by differences in instrumentation or resolution (as well as offering an additional opportunity to search for short term variability in 2004).

We supplemented these observations with 3 epochs of spectroscopy obtained with the Magellan Inamori Kyocera echelle spectrograph in 2009 June and July and 2010 July (see Cottaar et al. 2012) that have similar resolving power to the UVES data. Additional, lower resolution data include two NTT/EMMI spectra from 2002 and 2003 presented and described in Clark et al. (2005) and Negueruela & Clark (2005) respectively, a single spectrum from the ESO 1.52 m (Clark et al. 2005) and the original low signal to noise classification spectrum of Westerlund (1987) which was obtained in 1981 and hence extends the baseline of observations to three decades. Finally, we make use of the *K*-band spectrum presented by Mengel & Tacconi-Garman (2007; Table 1) obtained with the VLT/ISAAC on 2006 March 11 and, at longer wavelengths, a mid-IR spectrum obtained with the Infrared Space Observatory (ISO) Short Wavelength Spectrometer (SWS; de Graauw et al. 1996) on 1998 February 6 and taken from the database of Sloan et al. (2003).

3. Spectroscopy

Wd1-9 displays a very rich *R*- and *I*-band (~5800–9300 Å) emission line spectrum (Figs. 1 and 2) with a complete absence of any apparent photospheric absorption lines; the only absorption lines visible in the spectrum of Wd1-9 are interstellar lines of Na I and K I, strong diffuse interstellar bands at 6281, 6614, 8620 and 8648 Å (cf. Negueruela et al. 2010a), and telluric bands. Along with very strong emission lines of H, He I and O I λ8446, there are many permitted lines from neutral and singly-ionized metals, including N I, O I, Mg I, Mg II, Fe II, Ca II and Si II, and forbidden lines of [O I], [O II], [N II], [Fe II], [Ni II], [Ni III], [S III] and [Ar III]. Weak lines of C I, C II and [Fe III] are also observed, and S I, Ne I, N II, Al II, [Cr II] and [Ar IV] are tentatively identified. No compelling evidence for the presence of higher-excitation lines over this wavelength range is seen, with N IV λ7114 and He II λ1.012 μm absent in the UVES spectra.

At longer wavelengths, the *K*-band spectrum of Wd1-9 reported by Mengel & Taconni-Garman (2007) is essentially featureless, lacking the CO bandhead emission that is seen in many other sgB[e] stars (e.g. Liermann et al. 2010); the ~6159 Å TiO bandhead is likewise missing at shorter wavelengths. Wd1-9 is also not identified as an emission line object in He II(2.189 μm)-*continuum* or He II(1.012 μm)-*continuum* interference filter photometry (Crowther et al. 2006b; Groh et al. 2006). At mid-IR wavelengths Wd1-9 has a rich emission line spectrum superimposed on a continuum dominated by warm dust (Fig. 3 and Sect. 4). Various hydrogen lines are present as are a number of forbidden lines from species such as [Ar II], [Ar III], [Ne II], [Ne III], [S III], [S IV] and [O IV].

3.1. Hydrogen

The dominant feature in the R-band spectrum of Wd1-9 is an extremely strong Hα line ($EW = -640 \pm 40$ Å) with a relatively narrow core ($FWHM \sim 125$ km s^{-1}) and broad electron scattering wings extending to $\pm$1500 km s^{-1}, which appear asymmetric, with excess emission in the blue wing (Fig. 4). The Paschen series is seen in emission to $n = 35$, with the unblended Pa9...16 lines yielding a radial velocity (RV) of -28.9 ± 0.8 km s^{-1} that varies by less than 1 km s^{-1} in the three epochs of UVES data. Both Hα and the Paschen series lines appear to be marginally blueshifted in the 2004 FORS2 spectra, with a mean radial velocity -41 ± 2 km s^{-1} derived for the Pa9...16 lines.

[1] http://www.eso.org/sci/software/pipelines

[2] IRAF is distributed by the National Optical Astronomy Observatories, which are operated by the Association of Universities for Research in Astronomy, Inc., under cooperative agreement with the National Science Foundation.

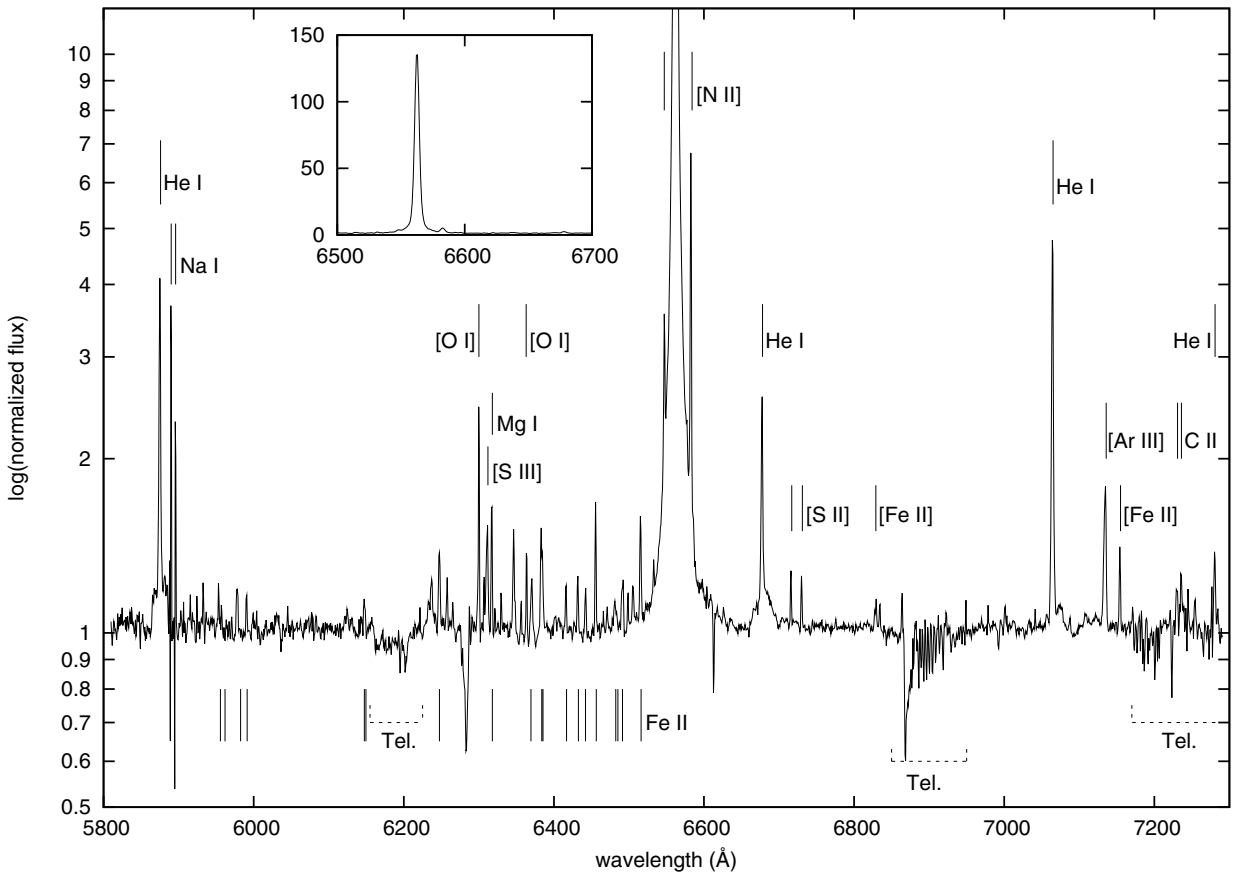

Fig. 1. Semi-logarithmic VLT/FORS2 spectrum from 2004 covering 5800–7300 Å. Rest wavelengths of the principal emission lines are indicated, and telluric bands are also identified. The low-resolution *inset* shows a linear plot of the 6500–6700 Å region to highlight the strength of the Hα emission.

Comparison with the FORS2 spectrum from 2011 suggests that this is not just an effect of the greatly improved resolution of the UVES data, although the relatively low resolution of the earlier dataset preclude detailed analysis.

At longer wavelengths, the ISO-SWS spectrum shows emission from Br$\alpha+\beta$, Pf$\alpha+\beta$, Hu$\alpha+\beta$ and the H7α and H8α transitions, although these lines are much diminished by continuum emission from hot dust (Fig. 3).

3.2. Helium

Strong He I emission is seen from the triplet He I $\lambda\lambda$5876,7065 and singlet He I λ6678 lines, while a weak He I λ7281 line and very weak I-band recombination lines from higher levels are also observed. The He I lines show the same blue-wing excess as the Hα and Paδ lines, but also display broad emission bases extending to at least $\pm$800 km s^{-1} that are plotted in Fig. 5 (see also Clark et al. 2008). The profile of the base is broadly consistent between UVES and FORS2 spectra, although the feature appears more pronounced at high velocities in the 2011 data; its presence in both datasets suggests it is both real and not a transient phenomenon. To the best of our knowledge these composite profiles are not observed in any other sgB[e] star, although LHA 120-S 134 does demonstrate weak, broad He IIλ4686 emission (Zickgraf et al. 1986).

3.3. Iron

A large number of Fe II lines are visible in the spectrum of Wd1-9, although no permitted lines of Fe I or Fe III are identified. Fe II λ9997 line is the most pronounced transition within our spectral coverage, while Fe II $\lambda\lambda$8490,8927,9203 lines are also strong. These lines originate from multiplets at $\sim$11 eV, implying strong Lyα pumping from metastable lower energy levels (Hamann & Simon 1986; Sigut & Pradhan 2003). The Fe II lines display an asymmetric profile (Fig. 4), with a strong, narrow red peak at -20 km s^{-1} and a broad blue flank with a sharp cutoff at -80 km s^{-1}. Lines from multiplets 40 and 74 (e.g. Fe II $\lambda\lambda$6456,6515; upper energy levels $\sim$5–6 eV) also show a distinct second peak at -50 km s^{-1} that is absent in the Lyman-pumped lines.

A number of [Fe II] lines are present, with [Fe II] λ7155 being the strongest; this line also having a relatively high critical density of $\sim10^8$ cm^{-3} (Zickgraf 2003). The blue flank of [Fe II] λ7155 is identical to the permitted Fe II lines, while the red peak is less pronounced and significantly narrower (Fig. 4). Two weak [Fe III] lines from multiplet 8F are also identified in the optical spectra[3]. In contrast to [Fe II] λ7155, [Fe III] λ8838 demonstrates a wedge-shaped profile, with a sharp red cut-off at $\sim$0 km s^{-1} and emission extending to almost -200 km s^{-1}.

3.4. CNO elements

Wd1-9 displays an extremely strong O I λ8446 emission line that has a similarly asymmetric profile to those of the strong Paschen-series lines, and strong O I λ7774 emission that displays a triple-peaked profile as a result of the partial resolution of three

[3] Other [Fe III] lines that might be strong in Wd1-9 lie too far bluewards to be accessible with the high reddening towards Wd1.

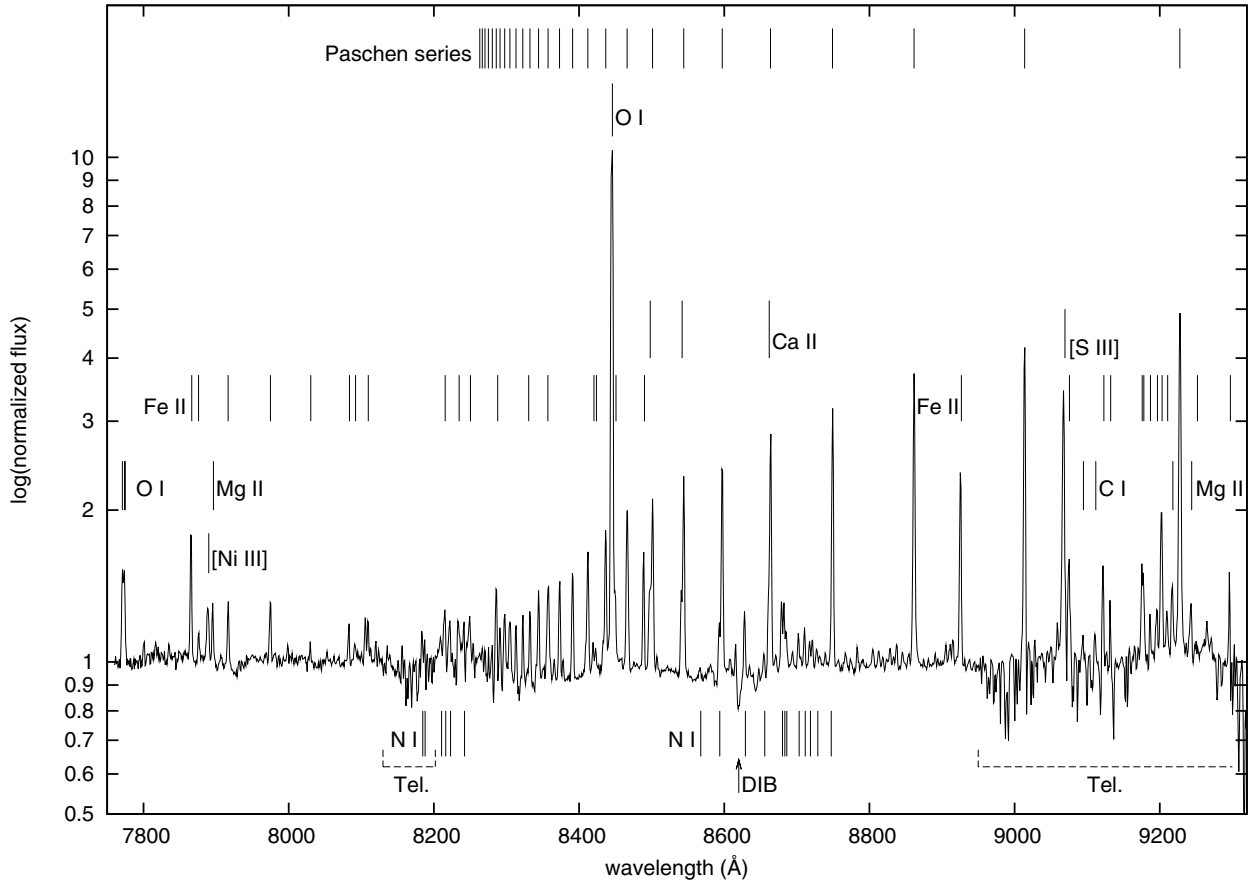

Fig. 2. Semi-logarithmic VLT/FORS2 spectrum from 2004 covering 7750–9300 Å. Rest wavelengths of the principal emission lines are indicated, and telluric bands are also identified. Note that O I λ8446 is saturated in this spectrum; the line reaches ~35× the continuum level in unsaturated spectra.

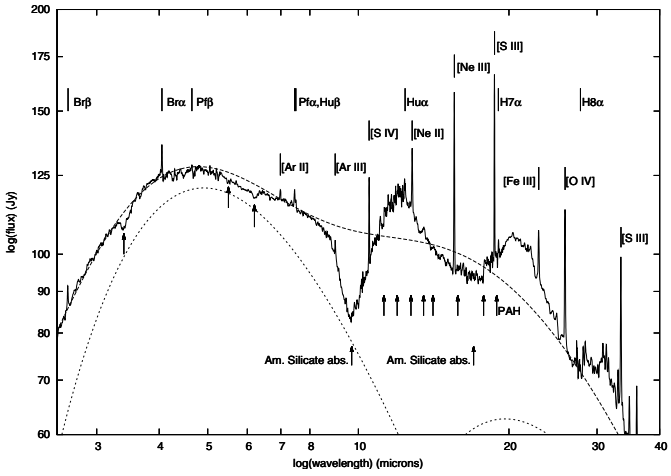

Fig. 3. Log-scaled ISO-SWS spectrum of Wd1-9 covering 2.4–20 μm. Rest wavelengths of the principal emission lines and interstellar features are indicated, with the arrowed features <6 microns being interstellar C2 and the PAH identifications from Boersma et al. (2010). An illustrative three-component black body fit comprising a stellar source (25 kK; not shown for clarity), hot (~1050 K) and cool (~260 K) dust (short dashed lines) and the summation of the contributions (long dashed line) is also shown.

component lines separated by ~3.5 Å. The ratio λ8446/λ7774 ~ 20 implies that Lyβ fluorescence in a dense, predominantly neutral transition zone between H I and H II regions is responsible for the O I λ8446 emission (Grandi 1980; Kwan 1984), with the O I λ7774 emission resulting from collisional excitation from the metastable $3s^5S^\circ$ quintet ground state; a number of weaker O I lines from higher quintet levels are also observed. In the 2011 data [O I] λ6300 is weak and has a radial velocity comparable to the other permitted lines, while [O I] λ6363 is almost absent, but in the 2004 data both lines are much stronger, with asymmetric profiles and redshifts of ~40 km s^{-1} compared to the Paschen series (Fig. 6).

The [O II] $\lambda\lambda$7319,7330 lines are present and display similar wedge-shaped profiles to [Fe III] λ8838. While heavy contamination by a telluric band precludes detailed analysis, the feature appears broader than the [O I] emission lines (Sect. 5). Finally [O IV] emission is observed in the mid-IR spectrum. This is the highest-excitation feature in our spectra and we discuss this further below.

N I lines from multiplets 1, 2 and 8 are seen in the *I*-band spectrum, while N II may also be present, but cannot be identified with certainty due to blending. The N I lines display near-identical profiles to Fe II, with line intensity ratios of the N I multiplet 1 lines suggesting they are optically thick (Hamann & Simon 1986). Strong [N II] $\lambda\lambda$6548,6582 emission is also present, with double peaked line profiles that appear to have weakened between 2004-11. Weak [C I] λ6588 and [C I] $\lambda\lambda$9094,9111 lines are also detected, with a profile similar to N I, while broad, weak C II $\lambda\lambda$7231,7236 lines are also present, although heavily blended with a telluric feature.

It appears likely that the N I and C I lines form in a cool dense environment. The N I multiplet 1 and 2 and C I multiplet 3 lines originate from excited states that are linked to the ground state

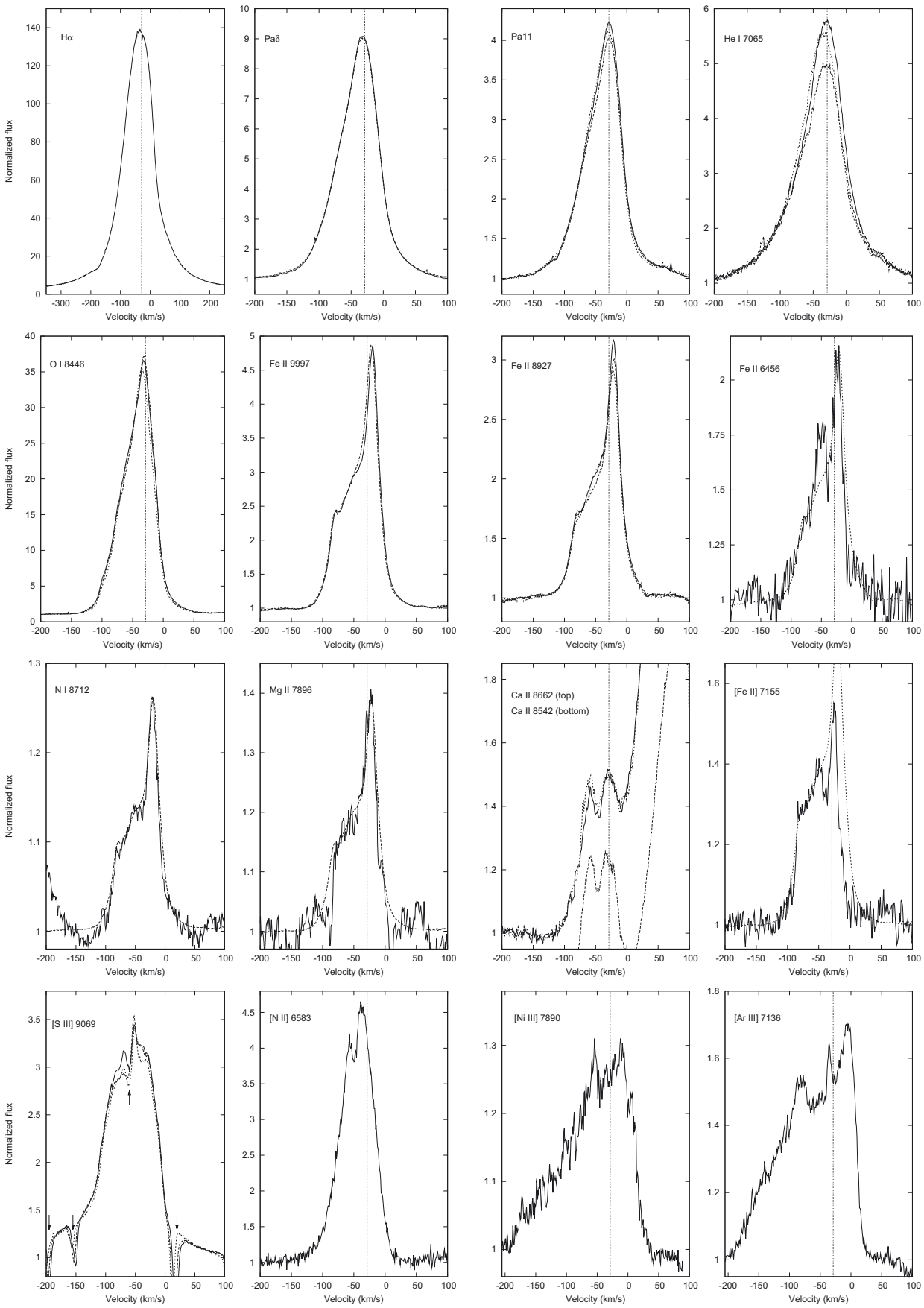

Fig. 4. Strong permitted and forbidden emission lines in the spectrum of Wd1-9. Note that the Hα (*top left*) has a different velocity scale to the remaining lines. In panels where multiple spectra are overplotted, solid line =6/4/2011, dashed line =14/4/2011 and dotted line =25/4/2011 respectively. For N I λ8712, Mg II λ7896, Fe II λ6456 and [Fe II] λ7155 a scaled Fe II λ9997 line is overplotted for comparison, and in all panels the vertical line marks the radial velocity derived from the Pa9...16 lines. Arrows mark telluric features overlapping the [S III] line.

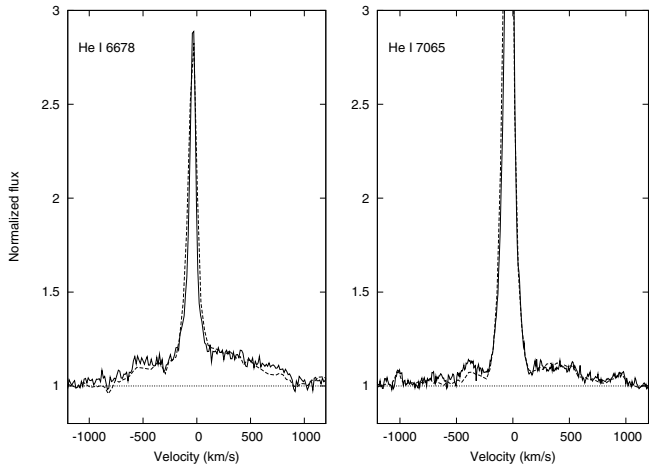

Fig. 5. He I $\lambda\lambda$6678,7065 from UVES (solid line) and 2004 FORS2 (dashed line), showing the broad bases to the lines.

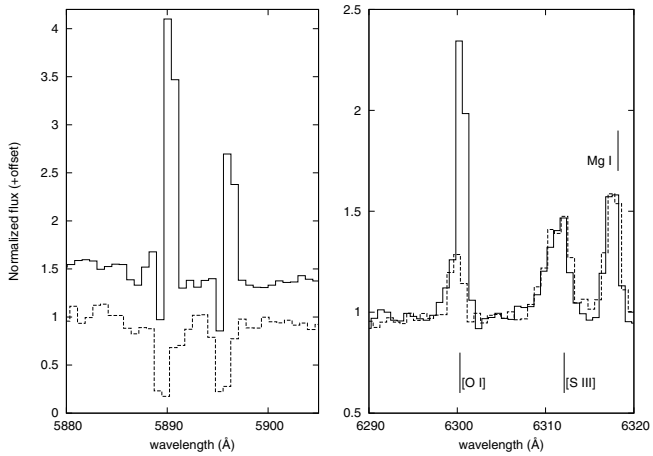

Fig. 6. Comparison FORS2 spectra from 2004 (solid line) and 2011 (dashed line), for Na I $\lambda\lambda$5890,5896 (*left panel*) and [O I] λ6300 (*right panel*).

by strong UV resonance lines and in a high density environment ($\geq 10^{10}$ cm^{-3}) the resonance lines become very optically thick (Hamann & Simon 1988), allowing the population of excited states to become large; collisional excitation can then populate the upper energy levels of the observed emission lines. In contrast, the [N II] lines have low critical densities ($<10^5$ cm^{-3}) and must therefore trace a physically distinct lower-density region.

3.5. Sodium and calcium

Na I and Ca II emission lines all arise from low-excitation states, implying the presence of a cool region shielded from the ionizing flux responsible for the Lyman-pumped lines. In the 2004 FORS2 data strong Na I $\lambda\lambda$5980,5986 emission lines were present, redshifted by ~40 km s^{-1} compared to the other permitted lines. Strong interstellar absorption bluewards of the emission line centre gives the lines apparent P Cygni profiles at this time, but the emission component is completely absent in the corresponding 2011 data, with only the interstellar components remaining (see Fig. 6; mirroring the behaviour of [O I]). Ca II $\lambda\lambda$8498,8542,8662 lines lie on the blue wing of adjacent Paschen-series lines and cannot be separated in the 2004 FORS2 spectrum, but are clearly resolved by UVES, showing double-peaked profiles separated by 26 km s^{-1} (Fig. 4); these lines are the only permitted lines to show clear double peaks. The corresponding [Ca II] $\lambda\lambda$7291,7324 lines that link the lower levels of the near-IR permitted lines to the Ca II ground state are not apparent, implying $n_e > 10^7$ cm^{-3} in the Ca II line forming region.

3.6. Forbidden lines

In addition to the forbidden line emission described above, strong [S III] $\lambda\lambda$9069,9531 lines were observed, along with [Ni II] $\lambda\lambda$7378,7412, [Ni III] $\lambda\lambda$7890,8500, [Ar III] $\lambda\lambda$7136,7751, and [S III] λ6312. Very weak [S II] λ1.287,1.320 μm and [Cr II] λ8125 lines are tentatively detected in the UVES spectrum; [Ar IV] λ7237 may be also be present, but is blended with a telluric band.

The observed lines span a range of ionziation energies and critical densities, indicating that they do not trace a single line-formation region, and this is reflected in their profiles. [Ni II] $\lambda\lambda$7378,7412 lines are weak but clearly double peaked with a separation ~25 km s^{-1}, resembling Ca II in this respect. In contrast the higher excitation [Ni III] λ7890,8500 and [Ar III] $\lambda\lambda$7136,7751 lines resemble the wedge-shaped profiles of [O II] $\lambda\lambda$7319,7330 and [Fe III] λ8838. [Ar III] displays a complex triple-peaked profile with narrow secondary components at −41 and −87 km s^{-1} superimposed on broad emission (Fig. 4) while [Ni III] only displays a single narrow component at −54 km s^{-1}. Finally [S III] λ9069 is very strong, and appears generally similar to [N II] but with a broader profile, complex peak structure and wings extending to at least −200/+100 km s^{-1}.

The ISO-SWS spectrum displays a number of strong fine-structure lines that include [Ar II], [Ar III], [Ne II], [Ne III], [S III], [S IV] and the aforementioned [O IV]. Emission in [Ne III], [S IV] and [O IV] suggest rather higher temperatures, with 41eV required to ionize Ne^+ and 54eV required to ionize O^{++}. These lines would require an ionising source with temperature ~60–80 kK, but this hard to reconcile with the lack of He II or N IV emission. However [O IV] emission also arises in post-shock gas with $n_e \sim 10^3$ cm^{-3} and $T \sim 50$ kK (Lutz et al. 1998) and we consider this a more likely origin for the highest-excitation forbidden lines visible in the ISO-SWS spectra.

3.7. Variability

Despite the presence of rapid aperiodic photometric variability (Bonanos 2007) and the inference from radio observations of a significantly higher mass loss rate in the past (Dougherty et al. 2010), one of the remarkable features of the current dataset is the lack of spectroscopic variability across the course of the 30 years of observations. This stands in contrast to other sgB[e] stars such as LHA 115-S 18 and luminous evolved stars in general (e.g. Clark et al. 2010, 2013); Wd1-9 shows no evidence of the long-term changes in gross spectral morphology characteristic of LBVs and cool hypergiants, although the sgB[e] star LHA 115-S 65 likewise demonstrated no variability for 3 decades before the sudden appearance of CO bandhead emission (Kraus et al. 2010; Oksala et al. 2012).

He I λ7065 is the *only* line in our spectra to show the significant short-term variability in strength – but not in radial velocity – that is characteristic of emission lines in other luminous early-type stars as a result of their asymmetric and unstable winds[4]. Apart from this, only the low excitation

[4] He I $\lambda\lambda$5876,6678 are only observed in the single UVES spectrum using dichoric #1, so cannot be checked for variability.

Na I $\lambda\lambda$5890,5896, [O I] $\lambda\lambda$6300,6363 and [S II] $\lambda\lambda$6716,6730 and the higher excitation [N II]$\lambda\lambda$6548,6582 lines have been found to vary, being substantially weaker post-2004. Finally, we reitterate that with the single exception of the 2004 FORS2 spectrum we were unable to determine any RV changes in the system from analysis of the Pa9...16 lines; a conclusion also reached by Cottaar et al. (2012) from analysis of the strong emission lines of their spectra. We therefore conclude that Wd1-9 does not appear to demonstrate the reflex RV motion expected of a binary system in these transitions, although we have insufficient data to determine whether the strength of the He I λ7065 transition is periodically modulated.

4. The dusty circumstellar environment of Wd1-9

The ISO-SWS spectrum of Wd1-9 (Fig. 3) shows pronounced similarities to those of other sgB[e] stars such as R66 and R126, suggesting comparable circumstellar envelope compositions and geometries. Specifically, the comparatively flat mid-IR spectra of these stars are indicative of multi-temperature, silicate-rich circumstellar dust and stand in contrast to the much "bluer" spectra of normal mass-losing (red) supergiants (Kastner et al. 2006, 2010). An illustrative three-component black body fit to the spectrum of Wd1-9 is plotted in Fig. 3, comprising a ~25 kK stellar source[5] and two dust components with temperatures ~1050 K and ~260 K, and provides a close match to the overall IR spectrum. However, we caution that a series of silicate absorption and emission features in the 8–35 μm range (cf. Chiar & Tielens 2006) leads to uncertainty in the placement of the continuum level, particularly for the cool dust component.

The profile of the 9.7 μm absorption component is very similar to that present in the ISO-SWS spectra of the heavily interstellar reddened WC8-9 Wolf-Rayet stars WR98a and WR112 ($A_V \sim 9.9$ and 10.2 respectively; van der Hucht et al. 1996). The comparable reddening of Wd1 cluster members (mean $A_V \sim 10.4$; Negueruela et al. 2010a) leads us to suppose that the main contribution to this feature in Wd1-9 is also interstellar in origin, although we cannot exclude an additional circumstellar component. A number of weak hydrocarbon absorption features are present at 3.4 μm, 5.5 μm and 6.2 μm; these features are also likely to be interstellar, as other indicators of a carbon-rich dust chemistry within the Wd1-9 circumstellar environment are absent.

No discontinuity is apparent at the ~29 μm transition between ISO-SWS bands 3 and 4, implying that the cool dust component is not greatly extended[6] and mid-IR imaging also shows that dust is located close to Wd1-9 (Clark et al. 1998). Given this, we make use of the simple semianalytic irradiated disk model of Dullemond et al. (2001) to examine the geometry and distribution of dust around Wd1-9 in an identical manner to Kastner et al. (2006) in their analysis of the sgB[e] star R126.

The model is based on a flared disk with an inner "hole", with three disk regions: a hot, "puffed up" inner rim that is directly exposed to the stellar flux, a cool intermediate region that is in the shadow of the rim and an outer flared region that is again illuminated by the central star. The model does not include

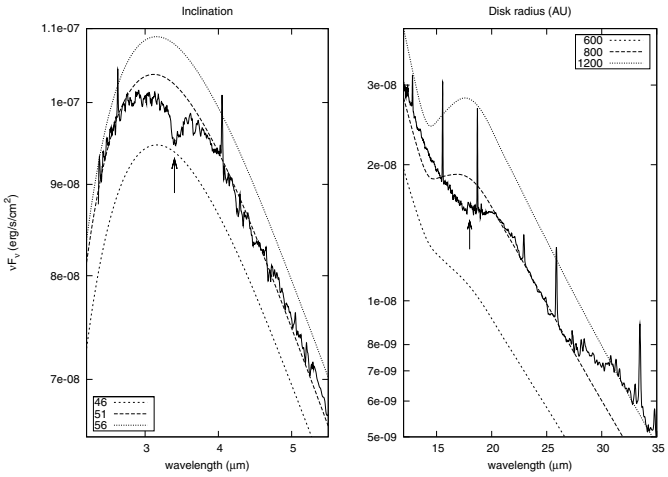

Fig. 7. Comparison of models for varying input parameters. *Left panel*: effect of varying inclination. *Right panel*: effect of varying the radius of the disk. Absorption features due to carbon (3.4 μm) and amorphous silicates (~18 μm) are marked.

the multi-dimensional radiative transfer required to fully model a dusty object like Wd1-9, nor the effect of interstellar absorption on the emergent spectrum and hence considerable caution must be employed in interpreting the results of this analysis in light of the preceding discussion. Nevertheless such an approach is useful in constraining the broad properties of the system and permits a direct comparison to be made to the disc properties of R126 (Kastner et al. 2006).

We fix the distance and luminosity of Wd1-9 at 5 kpc from Negueruela et al. (2010a), adopt $T_* = 25$ kK for the central source and, following Kastner et al. (2006), fix the hot dust temperature at 1050 K from the black-body fit to the short wavelength region of the spectrum. We find that the overall spectral energy distribution is reproduced well by the model, with inner and outer radii of ~60 AU and ~800 AU respectively, dust mass $\sim 4 \times 10^{-4}$ $M_\odot$ and inclination ~50 degrees (Fig. 7). The visibility of the hot inner wall of the disk represents the primary constraint on inclination, with both face-on and edge-on configurations showing weaker near-IR emission and a greater far-IR excess than intermediate viewing angles (see also Dullemond et al. 2001 on the effects of varying inclination). Similarly, the far-IR energy distribution depends on the extent of the cool outer reaches of the disk, with more compact configurations leading to lower emission beyond 20 μm due to the reduced emitting volume of cold dust; inconsistent with our observations. Subject to contamination by the assumed interstellar absorption features, the broad emission complexes at ~10 μm and ~20 μm (Fig. 3) are reproduced by optically thin emission from the surface layers of the disc, as found by Kastner et al. (2006; their Fig. 3) for R126.

Mindful of the limitations of our model, it is instructive to compare the results for Wd1-9 to those obtained by Kastner et al. (2006) for R126. As expected, given the similarities in the spectra, the dusty discs in both systems appear broadly comparable. However, that associated with Wd1-9 appears less massive than that of R126 in terms of dust mass (4×10^{-4} $M_\odot$ versus 3×10^{-3} $M_\odot$) and spatial extent ($r_{\rm out} \sim 800$ AU versus ~2500 AU), although it extends closer to the star ($R_{\rm in} \sim$ 60 AU versus ~120 AU) and hosts correspondingly hotter dust (~1050 K versus ~800 K). Nevertheless in both cases this is significantly lower than the expected dust sublimation temperature

[5] The fit is only weakly dependant on the choice of stellar temperature and a range corresponding to early- to mid-B supergiants can be accomodated.

[6] The ISO-SWS Band 3 aperture is $27 \times 14''$ while the Band 4 aperture is $33 \times 20''$; an extended cool component results in a discontinuity due to the inclusion of $\geq$30 μm emission from a region larger than the Band 3 aperture (Lamers et al. 1996).

(~1500 K), implying a central cavity. Given the isolation of R126, it is tempting to attribute the lower mass and size of the Wd1-9 disc to the harsher environment in which it resides due to the diffuse UV and X-ray radiation fields of Wd1. In this regard the commetary nebulae associated with the RSGs within Wd1 are also suggestive of ablation of their outer atmospheres by the action of the cluster wind/radiation field (Dougherty et al. 2010).

5. Wd1-9 as a sgB[e] star

Synthesising the results of the preceding sections, we may construct a picture of a highly structured and complex circumstellar environment associated with Wd1-9:

- A cool, dense (~5000 K, $>10^8$ cm^{-3}; Hamann & Simon 1988) region which is shielded from an ionising flux – and hence hydrogen neutral – in which the Ca II, C I, N I and Mg I form. The collisionally-excited Fe II lines with upper energy levels of ~5–7 eV would also arise here.
- A hotter, dense transitional zone between the H I and H II regions (~8000 K, 10^9–10^{10} cm^{-3}) where hydrogen is partially ionised (τ(Hα) > 10^3; Grandi 1980) in which Lyα pumping of Fe II and Lyβ pumping of O I λ8448 and Mg II proceeds.
- A hot H II region in which the H and He lines form.
- A relatively cool (>5000 K), low-density and velocity region where narrow singly-ionised forbidden lines of [Fe II], [O II] and [N II] form. The significant differences in critical densities for these lines (e.g. [Fe II]λ7155 versus [N II]λ6583) suggests that this region is itself structured.
- A hot, low density (~30 000 K, $<10^6$ cm^{-3}; Hamann & Simon 1988) region where relatively broad doubly ionised forbidden lines of [Ar III] and [S III] form.
- A high temperature, diffuse, post-shock region (~50 000 K, $n_e \sim 10^3$ cm^{-3}: Lutz et al. 1998) responsible for the highest excitation fine structure lines such as [O IV].
- A cool, massive dusty torus of radius ~60 to ~800 AU and mass $\sim 4 \times 10^{-2}$ $M_\odot$ assuming a canonical gas to dust ratio of 100.

And, including the results of previous studies, we may also add:

- A partially optically thick steady-state outflow with an r^{-2} density distribution and (unclumped) mass loss rate of $9.2^{+0.4}_{-0.5} \times 10^{-5}$ $M_\odot$ yr^{-1} (Dougherty et al. 2010).
- A compact H II region of inner radius 4000 AU indicative of enhanced mass loss ($33^{+12}_{-5} \times 10^{-5}$ $M_\odot$ yr^{-1}) which terminated ~200 yr ago (Dougherty et al. 2010).
- A region of very high temperature gas ($kT \sim 2.3^{+0.5}_{-0.3}$ keV; Clark et al. 2008).

The diversity observed in the line profiles also emphasises the complexity of the circumstellar environment (Fig. 4). On this basis, while we do not attempt to fully reconstruct the kinematics and geometry of the Wd1-9 system from these data, they do offer several additional insights. Firstly, no shell emission lines are present in the spectra, implying that Wd1-9 is not seen edge-on; consistent with the mid-IR modelling. No P Cygni profiles indicative of pure outflow are present in the hydrogen or helium lines, although the broad bases to He I$\lambda\lambda$5876, 6678 and 7065 are suggestive of a high velocity outflow. The remaining line profiles are harder to interpret. The asymmetries seen in the line profiles are common to B[e] stars and classical Be stars. In the latter objects they are attributed to the presence of global one armed oscillations in the gaseous circumstellar discs (e.g. Okazaki 1997); in sgB[e] stars one must also account for the presence of stellar or disc winds and self-absorption by the circumstellar disc/torus (Oudmaijer et al. 1998; Zickgraf 2003).

Nevertheless, the presence of double peaked emission lines in e.g. the Ca II and [Ni II] lines is suggestive of an origin in a quasi-Keplerian disc or torus (e.g. Kraus et al. 2010; Aret et al. 2012). Likewise the higher excitation permitted lines appear to be broader than the low excitation forbidden lines, as seen in other sgB[e] stars (Zickgraf 2003) and also consistent with this hypothesis. This is also apparent via comparison of the [O I] and [O II] lines, with the former narrower than the latter, as predicted for such a scenario by Kraus et al. (2013).

However, the asymmetric profiles of [O II]λ7319 and higher excitation species such as [Ni III]λ7890 and [Ar III]λ7136 also appear to show a departure from emission from an axisymmetric quasi-keplerian disc, due to the presence of an additional broad emission component. Somewhat surprisingly, a simple correspondence between line width and excitation does not appear to be present: e.g. [N II]λ6583 (excitation potential of 14.53 eV) is narrower than [Fe II]λ7155 (excitation potential of 7.9 eV). Indeed, in conjunction with excitation requirements and critical densities, comparison of the profiles of these lines (and also [Ar III]λ7136 versus [S III]λ9069) suggest that the physically distinct regions itemised above are themselves structured.

Wd1-9 therefore conforms well to the canonical picture of B[e] stars, with a dense, low-ionization equatorial region, possibly in quasi-Keplerian rotation, in which the low excitation permitted and forbidden lines form (Zickgraf et al. 1985, 2003; Lamers et al. 1998; Kraus et al. 2010; Aret et al. 2012). Higher-excitation lines appear to demonstrate an additional contribution which one might speculate arises in a radial outflow (stellar- or disc-wind?), while we may associate some lines (such as O I λ8446, [Fe II] λ7155 and the strong Lyα-pumped Fe II transitions) with a transitional zone on the surface of the disk, where densities are high but a significant ionizing flux is present. Finally, Wd1-9 appears encircled by a detatched massive dusty disc extending out to large radii.

6. The evolutionary state of Wd1-9

Presumably the result of the complete veiling of the "central engine" of Wd1-9 by circumstellar material, the absence of any photospheric features and apparent lack of RV changes indicative of orbital motion in Wd1-9 complicates its physical interpretation from optical spectroscopy. Consequently, the primary constraints on both the nature and evolutionary state of Wd1-9 come from radio (Dougherty et al. 2010) and X-ray observations (Skinner et al. 2006; Clark et al. 2008). The former implies a recent epoch of eruptive mass loss at rates significantly in excess of ~10^{-4} $M_\odot$ yr^{-1} that subsequently decreased by a factor of ~4 a few hundred years ago (Dougherty et al. 2010). Such extreme mass loss rates are found only in extreme cool hypergiants (Lobel et al. 2003; Humphreys et al. 2005), LBV outbursts (Davidson & Humphreys 1997; Groh et al. 2010) and the fast phases of Roche-lobe overflow in interacting binary stars (Langer et al. 2003; Petrovic et al. 2005), being ~2 orders of magnitude greater than expected for the late-O/early-B supergiants that characterise Wd1 at this time (Negueruela et al. 2010a; Crowther et al. 2006a).

The X-ray observations are potentially a more powerful diagnostic. The spectrum is best fitted by a thermal plasma model with $kT \sim 2.3$ keV, and yields a integrated luminosity of ~10^{33} erg s^{-1}; a combination of temperature and luminosity that is clearly inconsistent with emission from a single massive star (Clark et al. 2008). Therefore, despite the absence of

cyclic photometric or spectroscopic (RV) variability indicative of binarity, the X-ray luminosity and plasma temperature appear to require a colliding-wind system or a high-mass X-ray binary (HMXB).

X-ray detections of sgB[e] stars are rare (Bartlett et al., in prep.). Two bona fide HMXB with sgB[e] star primaries are known – CI Cam (e.g. Clark et al. 2000; Hynes et al. 2002) and IGR J16318-4848 (Filliatre & Chaty 2004) – while a dusty circumstellar environment has also been inferred for a further two – GX301-2 (Moon et al. 2007) and SS433 (Fuchs et al. 2006). While the X-ray luminosity of Wd1-9 is consistent with the first two systems (but is significantly fainter than the latter two) its thermal X-ray spectrum is very different from the hard, power law spectra of these HMXBs (Clark et al. 2008; Bartlett et al. 2013)[7].

In contrast to the HMXBs discussed above, Wd1-9 bears considerable resemblance in terms of both X-ray spectrum and luminosity to known compact, colliding wind binary systems within Wd1, such as the ($P_{\rm orb}\sim$)3-day WN7+O binary WR-B, the 4-day O+O binary Wd1-30a and the 7-day WN7b+OB binary WR-A (Bonanos 2007; Clark et al. 2008; Ritchie et al., in prep.). Indeed RV observations (Ritchie et al. 2009a, and in prep.) show that *all* OB supergiants within Wd1 with similarly hard X-ray spectra to Wd1-9 are binaries with periods less than ten days. A similarly short-period O6-7 V+O7–8 V progenitor system ($M_{\rm initial} \sim 40 + 35\ M_{\odot}$) for Wd1-9 would therefore fit both its current observational properties and the wider evolutionary context of Wd1 (cf. the eclipsing WNLh+O binary Wd1-13; Ritchie et al. 2010a).

If Wd1-9 is the short-period binary suggested by the X-ray data, it is not expected to undergo either an LBV or RSG phase. It will instead experience highly non-conservative mass transfer as the primary evolves off the MS and overflows its Roche lobe (Petrovic et al. 2005), leading to the ejection of the hydrogen envelope and direct formation of a very short period WR+O binary (cf. WR-B; Bonanos 2007) without the system undergoing a loop redwards across the Hertzsprung-Russell diagram (Clark et al. 2011). Theoretical models of massive binary evolution by Wellstein & Langer (1999) and Petrovic et al. (2005) indicate brief phases of *fast* Roche-lobe overflow mass loss at (time-averaged) rates $\gtrsim 10^{-4}\ M_{\odot}\,{\rm yr}^{-1}$; directly comparable to that inferred for Wd1-9 (Dougherty et al. 2010).

Following the fast phase of Roche-lobe overflow, mass loss rates decrease until either the surface hydrogen abundance of the primary drops below $X_{\rm s} \sim 0.4$ and a WR wind develops (Petrovic et al. 2005) or core hydrogen burning ends and a second phase of *fast* transfer takes place as the mass donor commences shell burning (Langer et al. 2003). Depending on how far mass transfer has progressed, both WRs and O9–B0 (super)giants therefore represent plausible current primaries for Wd1-9. A WC star is incompatible with the carbon-poor dust chemistry indicated by the infra-red observations, while an early WN star would display strong He II and N IV emission that is not apparent in our spectra. In contrast, the very weak photospheric lines of the interacting O+O binary Wd1-30a suggest that such a configuration would be completely undetectable against the rich emission line spectrum of Wd1-9, while weak He II emission from a WN9–11h+O system would also likely be undetectable. Such a system would ultimately emerge from the sgB[e] phase as an WNL+O binary, appearing similar to Wd1-13 (Ritchie et al. 2010a), WR-B (Bonanos 2007) and eventually, after further mass loss, WR-F (Clark et al. 2011). We therefore emphasise that if Wd1-9 is indeed a compact interacting binary, viable progenitor and descendent systems are present within Wd1.

[7] Two additional X-ray detections of Magellanic Cloud sgB[e] stars have been made (S18 and S134; Clark et al. 2013; Bartlett et al., in prep.) but low X-ray count rates preclude a determination of the nature of their putative binary companions.

6.1. Corrobarative evidence

6.1.1. Comparator systems

The suggestion that the B[e] phenomenon (in part) arises due to binary-driven mass loss is not new[8] and a number of lines of observational evidence/comparator systems support this assertion. Analogues of the detatched dusty toroid surrounding the central binary of Wd1-9 (Sect. 4) have been resolved interferometrically around the sgB[e] stars HD327083 (Wheelwright et al. 2012) and MWC300 (Wang et al. 2012), with the former of considerable interest since it comprises a binary within the torus. Although less massive and with larger orbital separation than expected for Wd1-9, GG Car and VFTS 698 are both spectroscopic sgB[e] binaries (Gosset et al. 1985; Dunstall et al. 2012), with the former associated with a circumbinary molecular disc/torus (Kraus et al. 2013). While not formally classified as a sgB[e] star, HDE 326823 is a likely ~6.123 day binary (Richardson et al. 2011), comprising a proto-WN8 primary (Marcolino et al. 2007) and a more massive secondary hidden by an accretion disc, with both stars in turn surrounded by a circumbinary disc with a dusty component (Ardila et al. 2010). Similarly RY Scuti is an 11-day eclipsing binary consisting of a Roche lobe-filling 8 $M_{\odot}$ O9.7 supergiant and 30 $M_{\odot}$ companion associated with a circumbinary disc ($r \sim 1$ AU) nested within a toroidal nebula ($r \sim 10^3$ AU), delineated by sequential radio and IR emission from ionised gas and warm dust (Smith et al. 2002, 2011; Grundstrom et al. 2007).

Given the similarity in evolutionary state of the latter two objects to that proposed for Wd1-9 a more detailed comparison is of interest. While a quantitative determination of the geometry of the circumstellar/-binary envelope of HDE 326823 has yet to be achieved, RY Scuti appears to differ from Wd1-9 in several aspects. Specifically, the inner bound of the (dust free) circumbinary disc in RY Scuti is over an order of a magnitude smaller than we infer for Wd1-9 (Sect. 4, Grundstrom et al. 2007); conversely the outer toroidal nebula of RY Scuti is significantly larger than the Wd1-9 dusty toroid. Given that the dust in the toroidal nebula of RY Scuti is already cooler than that found for Wd-9 and other sgB[e] stars (Kastner et al. 2006), it will not evolve into a similar sgB[e] configuration unless fresh dust production occurs in the inner circumbinary disc. A further difference is that the radio emission in Wd1-9 is associated with ongoing mass loss from the system, while in RY Scuti it arises from the detatched nebula. One might speculate that these discrepancies arise from differences in the mass-transfer pathways – and the stage of progression along them – experienced by both systems; the $\sim 25 + 15\ M_{\odot}$ initial configuration suggested for RY Scuti implies a lower mass than that of Wd1-9 (Smith et al. 2011 and Sect. 6.0) and consequently that mass transfer in RY Scuti may have proceded via a more conservative mode.

A better match to Wd1-9 may be provided by MWC349A. Binarity has been suggested by several studies (Hofmann et al. 2002; Gvaramadze & Menten 2012) and the circumstellar/-binary geometry appears similar to Wd1-9, comprising a warm,

[8] See for example Langer & Heger (1998), Sheikina (2000), Zickgraf (2003), Kastner et al. (2006, 2010), Miroshnichenko (2007), Kraus et al. (2012, 2013).

dusty Keplerian torus ($r \sim 100$ AU, $T \sim 600-1000$ K; Danchi et al. 2001; Kraemer et al. 2002; Weintroub et al. 2008) that is associated with a bipolar disc-wind visible at radio wavelengths (White & Becker 1985). Both Wd1-9 and MWC 349A also share similar optical and mid-IR spectra (Kraemer et al. 2002; Hamann & Simon 1988) and while the latter lacks the very high excitation lines and hard X-ray emission of the former, this might be the result of absorption by the dusty torus in MWC 349A, which is viewed edge on and hence obscures the central engine.

So to conclude; while we are able to identify a number of systems with features comparable to those of Wd1-9 we are not able to provide an exact match. However it appears that binary driven mass transfer can yield the defining observational features of the sgB[e] phenomenon and given the rapidity of this phase and the sensitivity of the process to initial conditions (e.g. component masses and orbital period; Petrovic et al. 2005) and indeed inclination, this is possibly unsurprising.

6.1.2. The association of sgB[e] stars with massive stellar clusters

A clear prediction of the hypothesis that a subset of sgB[e] stars form via binary interaction is that since the mass transfer phase is rapid ($\sim 10^4$ yr; Petrovic et al. 2005) such stars should be rare. Is this the case? An obvious methodology to assess this is to search for bona fide sgB[e] stars in young massive clusters, since this permits an accurate determination of stellar luminosity and also enables a direct comparison to the populations of other classes of massive stars[9]. The evolved stellar population of Westerlund 1 is certainly consistent with such an hypothesis; Wd1-9 is the only sgB[e] star amongst $\geq$100 OB supergiants and large numbers of other supposedly short lived objects such as hot and cool hypergiants and WR (Negueruela et al. 2010a; Ritchie et al., in prep.).

Spectroscopic surveys of massive stars are available for ~68 young ($\leq$20 Myr) stellar aggregates containing ~600 massive post-MS stars, enabling us to build upon this approach (Sect. A.1.). While evolved stars of all known spectral types are present within these clusters, only Wd1 and Cyg OB2 are found to host sgB[e] stars, while they are also the least frequently encountered post-MS stars in purely numerical terms (Table A.1). Trivially, these conclusions hold over any age subsets of the sample (for example RSG dominated clusters at >10 Myr). Turning to the Magellanic clouds, Massey et al. (2000) associate sgB[e] stars with two of the 19 MC clusters they study. LHA 120-S 134 appears a bona fide example and its spectral and X-ray properties point to it being a massive binary (Bartlett et al., in prep.). However Bonanos et al. (2009) question the identification of [L72] LH85-10 as a sgB[e] star, prefering a classical Be star classification on the basis of luminosity and shape of the IR continuum. Recently, four B[e] stars have been identified within the 30 Doradus star forming complex; VFTS 039, 698, 822 and 1003 (Evans et al. 2011 and in prep.). However, since star formation is still occurring within this non-coeval complex, distinguishing between sgB[e] and HerbigB[e] classifications for these stars is difficult, although, if CO bandhead emission is present, enrichment of ^{13}CO relative to ^{12}CO may in principle be used as a discriminant (Kraus 2009; Liermann et al. 2010). In any event, and as with Wd 1, with at most 4 candidates drawn from over 700 hot luminous stars (Doran et al. 2013) the stellar population of 30 Dor also argues for the intrinsic rarity of sgB[e] stars, as indeed do the dearth of clusters in both the Galaxy and Magellanic Clouds that host them.

If the B[e] phenomenon is an evolutionary state that *all* supergiants pass through (with progenitor masses spanning ~12 $M_\odot$ for the RSG clusters to ~100 $M_\odot$ for the Arches cluster) then the problem appears acute; the sgB[e] phase must be extremely brief, such that the chances of observation are low even in clusters containing a rich population of high-mass stars. In contrast, if the phenomenon is (in part) associated with rapid, binary-mediated mass transfer, then the absence of sgB[e] stars in these clusters is easier to understand: while still an intrinsically rapid process, in the youngest clusters only a limited subset of stars will be both compact binaries and sufficiently evolved to have reached the onset of mass transfer. While it might be supposed that the standard (Kroupa) initial mass function should lead to greater numbers of interacting binaries in the older, RSG dominated clusters, we suspect that the tendency towards conservative mass transfer in lower-mass systems (cf. Wellstein & Langer 1999) may preclude the extensive mass loss required to yield the sgB[e] phenomenon. Likewise, the huge physical extent of the RSGs that characterise these clusters means that such stars must be either isolated or in such wide binary systems that the secondary does not influence the evolution of the RSG primary[10].

7. Conclusions

A detailed synthesis of radio, infra-red, optical and X-ray observations of Wd1-9 are consistent with a hot, binary stellar source surrounded by a massive dusty disk viewed at moderate inclination. Suprisingly little evidence for long- or short-term spectroscopic variability is present at this time, despite apparent low-level aperiodic photometric modulation and historical indications of a long term evolution in the mass loss rate. Taken as a whole, the multiwavelength observational properties of Wd1-9 are consistent with those of other members of the rather heterogeneous class of sgB[e] stars, with the caveat that the presence of high excitation [Si IV] and [O IV] appears unprecedented. Nevertheless, the most likely explanation for their occurence – that Wd1-9 is a massive interacting binary and they are associated with shocked gas resulting from the wind/wind collision zone – is not without precendent (cf. LHA 115-S 18; Clark et al. 2013).

Due to the apparent lack of variability, no orbital period can be identified for Wd1-9; we suspect this is due to the almost complete veiling of the central binary by the circumstellar/-binary envelope. Nevertheless the X-ray properties of Wd1-9 provide a compelling case for binarity; all stars with comparable X-ray properties in Wd1 are confirmed O+O or WR+O colliding-wind binaries, with periods less than ten days (Ritchie et al. 2010b and in prep.). Of these, the 4-day interacting O+O binary W30a and the 7-day WN7+O binary WR-A have essentially identical X-ray spectra to that of Wd1-9 in terms of

[9] We note that in doing so we are implicitly associating the duration of rapid case A mass transfer with that of the sgB[e] phase. We are not aware of any studies regarding the lifetime of the dusty (Keplerian?) discs of sgB[e] stars, although following the analysis of Bik et al. (2006) regarding the photoevaporation of proto-stellar discs around OB stars and allowing for the additional effects of X-ray irradiation and a cluster UV radiation field one might expect them to be short-lived ($\lesssim 10^5$ yr).

[10] If sgB[e] stars were exclusively post-RSG objects one would anticipate their absence from clusters of this age, where stars are expected to end their lives as RSGs. However, the presence of low luminosity sgB[e] stars (e.g. $\log(L_{\rm bol}/L_*) < 5.0$; Gummersbach et al. 1995) implies that such comparatively low mass (<20 $M_\odot$) stars may indeed encounter this phase.

both morphology and luminosity. Crucially, if Wd1-9 is to be interpreted in terms of an ongoing or recently completed episode of binary-driven mass-transfer we are able to find both viable progenitor and descendant systems within Wd1 (Sect. 6).

While we cannot exclude the possibility that Wd1-9 is a quiescent HMXB, a more natural explanation for its observational properties is that it is a short-period O+O or WNVL+O binary that has recently undergone extreme mass loss during Roche-lobe overflow (Petrovic 2005), and is now buried within a circumbinary disk. Specifically, the extreme historical mass loss rate inferred from radio observations (Dougherty et al. 2010) is of a magnitude comparable with time averaged theoretical predictions for fast Roche-lobe overflow in Case A (core H-burning) binaries (Wellstein & Langer 1999; Petrovic et al. 2005). Likewise, our best-fit model to the spectral energy distribution of Wd1-9 is consistent with a detatched dusty torus surrounding the central engine, replicating the findings of Kastner et al. (2006), who interpreted this geometry in terms of a circumbinary Keplerian disc resulting from binary driven mass loss.

Critically, recent spectroscopic and interferometric observations have identified comparator short-period binary systems surrounded by detatched (dusty) discs (Sect. 6.1.1), while the apparent rarity of sgB[e] stars (Sect. 6.1.2) is also qualitatively consistent with the expected rapidity of mass-transfer in compact binaries ($\sim 10^4$ yr in its most extreme phase; Petrovic et al. 2005). We therefore suspect that binary interaction provides both a significant formation channel for evolved sgB[e] stars and a natural explanation for the large range of luminosities exhibited by such stars (e.g. Gummersbach et al. 1995; Miroshnichenko 2007; Aret et al. 2012). Indeed the apparently unbiased luminosity distribution of sgB[e] stars argues against their evolution from a mass-restricted subset of massive stars, in contrast to the occurence of phases such as the cool hypergiants and WN7-9ha stars. The diversity of observational properties of sgB[e] stars would then result from a combination of the initial binary configuration – and hence precise mass transfer route followed – and time since interaction.

In any event, Wd1-9 provides us with a unique opportunity to observe such a binary apparently "caught in the act", with the rich stellar population of its host cluster allowing us to place the system in a proper evolutionary context. As such it is likely to become a cornerstone system for quantitatively constraining the physical process of rapid binary-driven mass-transfer in massive evolved stars.

Acknowledgements. We thank Michiel Cottaar for providing spectra of Wd1-9 obtained in August 2009 and July 2010. J.S.C. gratefully acknowledges the support of an RCUK fellowship. I.N. has been funded by grant AYA2010-21697-C05-05 from the Spanish Ministerio de Ciencia e Innovación (MICINN).

References

Aidelman, Y., Cidale, L. S., Zorec, J., & Airas, M. L. 2012, A&A, 544, A64
Ankay, A., Kaper, L., de Bruijne, J. H. J., et al. 2001, A&A, 370, 170
Appenzeller, I., Fricke, J, Fürtig, W., et al. 1998, The Messenger, 94, 1
Ardila, D. R., Van Dyk, S. D., Makowiecki, W., et al. 2010, ApJS, 191, 301
Aret, A., Kraus, M., Muratore, M. F., & Borges Fernandes, M. 2012, MNRAS, 423, 284
Barbon, R., Carraro, G., Munari, U., Zwitter, T., & Tomasella, L. 2000, A&AS, 144, 451
Bartlett, E. S., Clark J. S., Coe, M. J., Garcia, M. R., & Uttley, P. 2013, MNRAS, 429, 1213
Baume, G., Vázquez, R. A., Carraro, G., & Feinstein, A. 2003, A&A, 402, 549
Bibby, J. L., Crowther, P. A., Furness, J. P., & Clark, J. S. 2008, MNRAS, 386, L23
Bik, A., Kaper, L., & Waters, L. B. F. M. 2006, A&A, 455, 561
Blum, R. D., Damineli, A., & Conti, P. S. 1999, AJ, 117, 1392
Boersma, C., Bauschlicher, C. W., Allamandola, L. J., et al. 2010, A&A, 511, A32
Bonanos, A. Z. 2007, AJ, 133, 2696
Bonanos, A. Z., Massa, D. L., Sewilo, M., et al. 2009, AJ, 138, 1003
Borgman, J., Koornneef, J., & Slingerland, J. 1970, A&A, 4, 248
Borissova, J., Ivanov, V. D., Hanson, M. M., et al. 2008, A&A, 488, 151
Borissova, J., Georgiev, L., Hanson, M. M., et al. 2012, A&A, 546, A110
Bosch, G., Barba, R., Morrell, N., et al. 2003, MNRAS, 341, 169
Brandner, W., Grebel, E. K., Chu, Y.-H., & Weis, K. 1997, ApJ, 475, L45
Chené A.-N., Borissova, J., Bonatto, C., et al. 2013, A&A, 549, A98
Chiar, J. E., & Tielens, A. G. G. M. 2006, ApJ, 637, 774
Clark, J. S., Fender, R. P., Waters, L. B. F. M., et al. 1998, MNRAS, 299, 43
Clark, J. S., Miroshnichenko, A. S., Larionov, V. M., et al. 2000, A&A, 356, 50
Clark, J. S., Negueruela, I., Crowther, P. A., & Goodwin, S. 2005, A&A, 434, 949
Clark, J. S., Muno, M. P., Negueruela, I., et al. 2008, A&A, 477, 147
Clark, J. S., Negueruela, I., Davies, B., et al. 2009, A&A, 498, 109
Clark, J. S., Ritchie, B. W., & Negueruela, I. 2010, A&A, 514, A87
Clark, J. S., Ritchie, B. W., Negueruela, I., et al. 2011, A&A, 531, A28
Clark, J. S., Bartlett, E. S., Coe, M. J., et al. 2013, A&A, 560, A10
Cottaar, M., Meyer, M. R., Andersen, M., & Espinoza, P. 2012, A&A, 539, A5
Crowther, P. A., Lennon, D. J., & Walborn, N. R. 2006a, A&A, 446, 279
Crowther, P. A., Hadfield, L. J., Clark, J. S., Negueruela, I., & Vacca, W. D. 2006b, MNRAS, 372, 1407
Currie, T., Hernandez, J., Irwin, J., et al. 2010, ApJS, 186, 191
Danchi, W. C., Tuthill, P. G., & Monnier, J. D. 2001, ApJ, 562, 440
Davidson, K., & Humphreys, R. M. 1997, ARA&A, 35, 1
Davies, B., Figer, D. F., Kudritzki, R.-P., et al. 2007a, ApJ, 671, 781
Davies, B., Oudmaijer, R. D., & Sahu, K. C. 2007b, ApJ, 671, 2059
Davies, B., Figer, D. F., Law, C. J., et al. 2008, ApJ, 676, 1016
Davies, B., Figer, D. F., Kudritzki, R.-P., et al. 2009, ApJ, 707, 844
Davies, B., Clark, J. S., Trombley, C., et al. 2012a, MNRAS, 419, 1871
Davies, B., de La Fuente, D., Najarro, F., et al. 2012b, MNRAS, 419, 1860
De Becker, M., Rauw, G. Blomme, R., et al. 2005, A&A, 437, 1029
Dekker, H., D'Odorico, S., Kaufer, A., Delabre, B., & Kotzlowski, H. 2000, SPIE, 4008, 534
de Graauw, T., Haser, L. N., Beintema, D. A., et al. 1996, 315, L49
de La Fuente, D., Najarro, F., Davies, B., & Figer, D. F. 2013, in Highlights of Spanish Astrophysics VII, Proc. of the X Scientific Meeting of the Spanish Astronomical Society (SEA), eds. J. C. Guirado, et al., 534
Doran, E. I., Crowther, P. A., de Koter, A., et al. 2013, A&A, 558, A134
Dougherty, S. M., Clark, J. S., Negueruela, I., Johnson, T., & Chapman, J. M. 2010, A&A, 511, A58
Dullemond, C. P., Dominik, C., & Natta, A. 2001, ApJ, 560, 957
Dunstall, P. R., Fraser, M., Clark, J. S., et al. 2012, A&A, 542, A50
Eggenberger, P., Meynet, G., & Maeder, A. 2002, A&A, 386, 576
Evans, C. J., Smartt, S. J., Lee, J.-K., et al. 2005, A&A, 437, 467
Evans, C. J., Taylor, W. D., Hénault-Brunet, V., et al. 2011, A&A, 530, A108
Figer, D. F., McLean, I. S., & Morris, M. 1999, ApJ, 514, 202
Filliatre, P., & Chaty, S. 2004, ApJ, 616, 469
Fitzgerald, M. P., Luiken, M., Maitzen, H. M., & Moffat, A. F. J. 1979, A&AS, 37, 345
Fitzsimmons, A. 1993, A&AS, 99, 15
Fuchs, Y., Koch Miramond, L., & Ábrahám, P. 2006, A&A, 445, 1041
González-Fernández, C., & Negueruela, I. 2012, A&A, 539, A100
Gosset, E., Hutsemekers, D., Surdej, J., & Swings, J. P. 1985, A&A, 153, 71
Grandi, S. A. 1980, ApJ, 238, 10
Graus, A. S., Lamb, J. B., & Oey, M. S. 2012, ApJ, 759, 10
Groh, J. H., Damineli, A., Teodoro, M., & Barbosa, C. L. 2006, A&A, 457, 591
Groh, J. H., Nielsen, K. E., Damineli, A., et al. 2011, A&A, 517, A9
Groh, J. H., Meynet, G., Georgy, C., & Ekstrom, S. 2013, A&A, 558, A131
Grundstrom, E. D., Gies, D. R., Hillwig, T. C., et al. 2007, ApJ, 667, 505
Gummersbach, C. A., Zickgraf, F.-J., & Wolf, B. 1995, A&A, 302, 409
Gvaramadze, V. V., & Menten, K. M. 2012, A&A, 541, A7
Hamann, F., & Simon, M. 1986, ApJ, 311, 909
Hamann, F., & Simon, M. 1988, ApJ, 327, 867
Hanson, M. M. 2003, ApJ, 597, 957
Hanson, M. M., Kurtev, R., Borissova, J., et al. 2010, A&A, 516, A35
Harayama, Y., Eisenhauer, F., & Martins, F. 2008, ApJ, 675, 1319
Hillenbrand, L. A., Massey, P. Strom, S. E., & Merrill, K. M. 1993, AJ, 106, 1906
Hillier, D. J. 2006, in Stars with the B[e] phenomenon, ASP Conf. Ser., 355, 39
Hofmann, K.-H., Balega, Y., Ikhsanov, N. R., Miroshnichenko, A. S., & Weigelt, G. 2002, A&A, 395, 891
van de Hucht, K. A., Morris, P. W., Williams, P. M., et al. 1996, A&A, 315, L193
Humphreys, R. M., Davidson, K., Ruch, G., & Wallerstein, G. 2005, AJ, 129, 492
Hynes, R. I., Clark, J. S., Barsukova, E. A., et al. 2002, A&A, 392, 991

Kaltcheva, N., Gredel, R., & Fabricius, C. 2001, A&A, 372, 95
Kastner, J. H., Buchanan, C. L., Sargent, B., & Forrest, W. J. 2006, ApJ, 638, L29
Kastner, J. H., Buchanan, C., Saghai, R., Forrest, W. J., & Sargent, B. A. 2010, AJ, 139, 1993
Kharchenko, N. V., Piskunov, A. E., Roeser, S., Schilbach, E., & Scholz, R. D. 2005, A&A, 438, 1163
Kolaczkowski, Z., Pigulski, A., Kopacki, G., & Michalska, G. 2004, AcA, 54, 33
Kraemer, K. E., Sloan, G. C., Price, S. D., & Walker, H. J. 2002, ApJS, 140, 349
Kraus, M. 2009, A&A, 494, 253
Kraus, M., Borges Fernandes, M., & de Araújo, F. X. 2007, A&A, 463, 627
Kraus, M., Borges Fernandes, M., & de Araújo, F. X. 2010, A&A, 517, A30
Kraus, S., Calvet, N., Hartmann, L., et al. 2012, ApJ, 746, L2
Kraus, M., Oksala, M., Nickeler, D., et al. 2013, A&A, 549, A28
Kurtev, R., Borissova, J., Georgiev, L., Ortolani, S., & Ivanov, V. D. 2007, A&A, 475, 209
Kwan, J. 1984, ApJ, 283, 70
Lamers, H. J. G. L. M., Morris, P. W., Voors, R. H. M., et al. 1996, A&A, 315, 225
Lamers, H. J. G. L. M., Zickgraf, F.-J., de Winter, D., Houziaux, L., & Zorec, J. 1998, A&A, 340, 117
Langer, N., & Heger, A. 1998, Astrophys. Space Sci. Libr., 233, 235
Langer, N., Wellstein, S., & Petrovic, J. 2003, in A Massive Star Odyssey, from Main Sequence to Supernova, eds. K. A. van der Hucht, A. Herrero, & C. Esteban, IAU Symp., 212, 275
Liermann, A., Hamann, W.-R., & Oskinova, L. M. 2009, A&A, 494, 1137
Liermann, A., Kraus, M., Schnurr, O., & Fernandes, M. 2010, MNRAS, 408, L6
Liermann, A., Hamann, W.-R., & Oskinova, L. M., 2012, A&A, 540, A14
Lobel, A., Dupree, A. K., Stefanik, R. P., et al. 2003, ApJ, 583, 923
Lutz, D., Kunze, D., Spoon, H. W. W., & Thornley, M. D. 1998, A&A, 333, L75
Marco, A., & Negueruela, I. 2013, A&A, 552, A92
Marcolino, W. L. F., de Aruaújo, F. X., Lorenz-Martins, S., & Borges Fernandes, M. 2007, AJ, 133, 489
Martayan, C., Floquet, M., Hubert, A. M., et al. 2008, A&A, 489, 459
Martins, F., Genzel, R., Hillier, D. J., et al. 2007, A&A, 468, 233
Martins, F., Hillier, D. J., Paumard, T., et al. 2008, A&A, 478, 219
Massey, P., Johnson, K. E., & DeGioia-Eastwood, K. 1995, ApJ, 454, 141
Massey, P., Waterhouse, E., & DeGioia-Eastwood, K. 2000, AJ, 119, 2214
Massey, P., DeGioia-Eastwood, K., & Waterhouse, E. 2001, AJ, 121, 1050
Melena, N. W., Massey, P., Morrell, N. I., & Zangari, A. M. 2008, AJ, 135, 878
Mengel, S., & Tacconi-Garman, L. E. 2007, A&A, 466, 151
Messineo, M., Davies, B., Ivanov, V. D., et al. 2009, ApJ, 697, 701
Messineo, M., Figer, D. F., Davies, B., et al. 2010, ApJ, 708, 1241
Messineo, M., Davies, B., Figer, D. F., et al. 2011, ApJ, 733, 41
Michalska, G., Niemczura, E., Pigulski, A. Steślicki, M., & Williams, A. 2013, MNRAS, 429, 1354
Miroshnichenko, A. S. 2007, ApJ, 667, 497
Moon, D.-S., Kaplan, D. L., Reach, W. T., et al. 2007, ApJ, 671, L53
Morris, P. W., Eenens, P. R. J., Hanson, M. M., Conti, P. S., & Blum, R. D. 1996, ApJ, 470, 597
Muno, M. P., Clark, J. S., Crowther, P. A., et al. 2006, ApJ, 636, L41
Negueruela, I., & Clark, J. S. 2005, A&A, 436, 541
Negueruela, I., Marco, A., Herrero, A., & Clark, J. S. 2008, A&A, 487, 575
Negueruela, I., Clark, J. S., & Ritchie, B. W. 2010a, A&A, 516, A78
Negueruela, I., González-Fernández, C., Marco, A., Clark, J. S., & Martínez-Núñez, S. 2010b, A&A, 513, A74
Negueruela, I., González-Fernández, C., Marco, A., & Clark, J. S. 2011, A&A, 528, A59
Okazaki, A. 1997, A&A, 318, 548
Oksala, M. E., Kraus, M., Arias, M. L., et al. 2012, MNRAS, 426, L56
Oudmaijer, R. D., Proga, D., Drew, J. E., & de Winter, D. 1998, MNRAS, 300, 170
Pandey, A. K., Upadhyay, K., Ogura, K., et al. 2005, MNRAS, 358, 1290
Pasquini, L., Avila, G., Blecha, A., et al. 2002, The Messenger, 110, 1
Paumard T., Genzel, R., Martins, F., et al. 2006, ApJ, 643, 1011
Petrovic, J., Langer, N., & van der Hucht, K. A. 2005, A&A, 435, 1013
Podsiadlowski, P., Morris, T. S., & Ivanova, N. 2006, in Stars with the B[e] phenomenon, ASP Conf. Ser., 355, 259
Polcaro, V. F., & Norci, L. 1998, A&A, 339, 75
Ramsay, G., & Pollacco, D. L. 1992, A&AS, 94, 73
Rauw, G., Manfroid, J. Gosset, E., et al. 2007, A&A, 463, 981
Rauw, G., Sana, H., & Nazé, Y. 2011, A&A, 535, A40
Richardson, N. D., Gies, D. R., & Williams, S. J. 2011, AJ, 142 201
Ritchie, B. W., Clark, J. S., Negueruela, I., & Crowther, P. A. 2009a, A&A, 507, 1585
Ritchie, B. W., Clark, J. S., Negueruela, I., & Najarro, F. 2009b, A&A, 507, 1597
Ritchie, B. W., Clark, J. S., Negueruela, I., & Langer, N. 2010a, A&A, 520, A48
Ritchie, B. W., Clark, J. S., & Negueruela, I. 2010b, Bull. Soc. Roy. Sci. Liège, 80, 628
Sana, H., Gosset, E., Rauw, G., Sung, H., & Vreux, J.-M. 2006, MNRAS, 372, 661
Schnurr, O., Casoli, J., Chené, A.-N., Moffat, A. F. J., & St-Louis, N. 2008, MNRAS, 389, L38
Sheikina, T. A., Miroshnichenko, A. S., & Corporan, P. 2000, in The Be Phenomenon in Early-Type Stars, IAU Colloq. 175, eds. A. S. Myron, & F. H. Huib, ASP Conf. Ser., 214, 494
Shi, H. M., & Hu, J. Y. 1999, A&AS, 136, 313
Sigut, T. A. A., & Pradhan, A. K. 2003, ApJS, 145, 15
Skinner, S. L., Simmons, A. E., Zhekov, S. A., et al. 2006, ApJ, 639, L35
Slesnick, C. L., Hillenbrand, L. A., & Massey, P., 2002, ApJ, 576, 880
Sloan, G. C., Kraemer, K. E., Price, S. D., & Shipman, R. F. 2003, ApJS, 147, 379
Smartt, S. J., Lennon, D. J., Kudritzki, R. P., et al. 2002, A&A, 391, 979
Smith, N. 2006, MNRAS, 367, 763
Smith, N., Gehrz, R. D., Stahl, O., Balick, B., & Kaufer, A. 2002, ApJ, 578, 464
Smith, N., Bally, J., & Walawender, J. 2007, AJ, 134, 846
Smith, N., Gehrz, R. D., Campbell, R., et al. 2011, MNRAS, 418, 1959
Sowell, J. R. 1987, ApJS, 64, 241
Stothers, R. B., & Chin, C.-W. 1996, ApJ, 468, 842
Turner, D. G. 1973, AJ, 78, 597
Wang, J.-J., & Hu, J.-Y. 2000, A&A, 356, 118
Wang, Y., Weigelt, G., Kreplin, A., et al. 2012, A&A, 545, L10
Wellstein, S., & Langer, N. 1999, A&A, 350, 148
Weintroub, J., Moran, J. M., Wilner, D. J., et al. 2008, ApJ, 677, 1140
Westerlund, B. E. 1961, PASP, 73, 51
Westerlund, B. E. 1987, A&AS, 70, 311
Wheelwright, H. E., de Wit, W. J., Weigelt, G., Oudmaijer, R. D., & Ilee, J. D. 2012, A&A, 543, A77
White, R. L., & Becker, R. H. 1985, ApJ, 297, 677
Zhang, X. B., Luo, C. Q., & Fu, J. N. 2012, AJ, 144, 86
Zhu, Q., Davies, B., Figer, D. F., & Trombley, C. 2009, ApJ, 702, 929
Zickgraf, F.-J. 2003, A&A, 408, 257
Zickgraf, F.-J., Wolf, B., Stahl, O., Leitherer, C., & Klare, G. 1985, A&A, 143, 421
Zickgraf, F. J., Wolf, B., Stahl, O., Leitherer, C., & Appenzeller, I. 1986, A&A, 163, 119
Zickgraf, F.-J., Wolf, B., Stahl, O., & Humphreys, R. M. 1989, A&A, 220, 206

Pages 13 to 16 are available in the electronic edition of the journal at http://www.aanda.org

Table 1. Journal of observations.

Date	MJD[a]	Instrument	Mode	Wavelength range	Reference
24/06/1981	44 779	ESO 3.6 m/B&C	–	~6500–8700 Å	Westerlund (1987)
06/02/1998	50 850	ISO/SWS	AOT1, speed 1	2.38–45.20 μm	This work
24/06/2001	52 084	ESO 1.52 m + B&C	Loral#38, GRAT#1	6000–10 500 Å	Clark et al. (2005)
07/06/2002	52 432	NTT/EMMI	REMD (2x2) + GRAT#7	6310–7835 Å	Clark et al. (2005)
06/06/2003	52 796	NTT/EMMI	REMD (2x2) + GRAT#6	8225–8900 Å	Negueruela & Clark (2005)
12/06/2004	53 168	VLT/FORS2	longslit (0.3″) + G1200R	5750–7310 Å	Negueruela et al. (2010a)
13/06/2004	53 169	VLT/FORS2	longslit (0.3″) + G1200R	5750–7310 Å	Negueruela et al. (2010a)
14/06/2004	53 170	VLT/FORS2	longslit (0.3″) + G1028z	7730–9480 Å	Negueruela et al. (2010a)
14/06/2004	53 170	VLT/FORS2	longslit (0.3″) + G1200R	5750–7310 Å	Negueruela et al. (2010a)
11/03/2006	53 805	VLT/ISAAC	SWS(MR)	22490–23 730 Å	Mengel & Tacconi-Garman (2007)
13/06/2009	54 969	Magellan Clay/MIKE	0.7″ slit	3200–9000 Å	Cottaar et al. (2012)
10/07/2009	55 023	Magellan Clay/MIKE	0.7″ slit	3200–9000 Å	Cottaar et al. (2012)
10/07/2010	55 388	Magellan Clay/MIKE	0.7″ slit	3200–9000 Å	Cottaar et al. (2012)
06/04/2011	55 657	VLT/UVES	CD#4 (860) + IMSL1	6708–10 426 Å	This work
14/04/2011	55 665	VLT/UVES	CD#4 (860) + IMSL1	6708–10 426 Å	This work
16/04/2011	55 667	VLT/FORS2	longslit (0.3″) + G1028z	7730–9480 Å	This work
16/04/2011	55 667	VLT/FORS2	longslit (0.3″) + G1200R	5750–7310 Å	This work
17/04/2011	55 668	VLT/FLAMES	GIRAFFE + HR21	8484–9001 Å	This work
25/04/2011	55 676	VLT/UVES	CD#4 (760) + IMSL1	5708–9464 Å	This work
22/05/2011	55 703	VLT/FLAMES	GIRAFFE + HR21	8484–9001 Å	This work
24/06/2011	55 736	VLT/FLAMES	GIRAFFE + HR21	8484–9001 Å	This work

Notes. [(a)] Modified Julian date at the start of the integration.

Appendix A: Summary of the evolved stellar content of Galactic young massive clusters

In order to determine the relative frequency of occurence of sgB[e] stars in comparison to other post-MS sub-types we constructed a representative census of well-studied young (≤20 Myr), massive Galactic clusters. To accomplish this we employed the source lists of Massey et al. (1995, 2001), Eggenberger et al. (2002), Crowther et al. (2006b), Evans et al. (2011), Davies et al. (2012b) and Chené et al. (2013) to undertake a literature survey[11], supplemented with the 3 Galactic Centre clusters and a number of aggregates associated with Giant H II regions[12]; as expected the latter possessed no unambiguous post-MS stars and so are not considered further. This resulted in a total of ∼68 stellar clusters and/or associations and where possible we present both cluster mass and age in Table A.1, along with associated uncertainties if quoted in the literature.

For simplicity we group stars into eight broad spectral classifications in Table A.1, based on our current understanding of the evolutionary sequence of post-MS stars; a more detailed breakdown is superfluous, given our simple aim of qualitatively determining the rarity, or otherwise, of sgB[e] stars. This results in a total of ≳600 stars.

Inevitably both the cluster census and the populations of individual clusters summarised in Table A.1 are likely to be incomplete and subject to observational biases that are difficult to quantify given the diverse detection strategies employed by the various authors; hence we consider the values quoted to be lower limits. Specifically:

- The location of RSGC1-6 within a wider star forming region similarly dominated by RSGs complicates assessment of cluster extent/membership. Moreover, interstellar extinction mandates their study in the far-red/near-IR, biasing any surveys against the detection of blue supergiants and WRs, noting that population synthesis arguements would suggest broadly comparably numbers of blue and red supergiants in 10–20 Myr-old clusters (e.g. Davies et al. 2009).
- More generally, the lack of systematic narrow-band imaging surveys for obscured clusters will hamper identification of intrinsically faint WRs, while the weak winds of lower-luminosity OB supergiants will not yield pronounced emission lines and hence will prevent their detection via such an observational strategy. We suspect that the second limitation is particularly problematic for the Galactic Centre proper and Quintuplet clusters, and is further compounded by the low S/N of available spectra for the latter aggregate, to the extent that in many cases we are unable to confidently determine accurate spectral types and/or luminosity classes for individual members (Figer et al. 1999; Liermann et al. 2009).
- Any single-epoch observational survey will be biased against identifying LBVs; one might anticipate that both late-B supergiants and YHGs could be cool-phase LBVs.
- The qualitative classification criteria used to distinguish between yellow super- and hyper-giants.

Nevertheless we suspect that sgB[e] stars will be amongst those least affected by incompleteness; their strong emission lines, intrinsic brightness and characteristic near- to mid-IR excess (e.g. Bonanos et al. 2009) render them easily identifiable. While we recognise the overlap in spectral morphologies of sgB[e] stars and cool-phase LBVs in the near-IR window (cf. S18 and GG Car versus AG Car; Morris et al. 1996) comparison of both near- and mid-IR colours allows for their separation (Zickgraf et al. 1986; Bonanos et al. 2009). Moreover, they may be distinguished from the spectroscopically similar but less evolved Herbig AeBe stars on the basis of their intrinsic luminosities.

Bearing the above caveats in mind, the results of this compilation appear broadly as expected (cf. Davies et al. 2009), with younger clusters being dominated by the apparently massive core H-burning early-mid O supergiants and WNLha stars and older clusters hosting increasing numbers of RSGs. Both WN and WC subtypes are present in young (<10 Myr) clusters; it is curently not possible to determine whether their absence in older clusters is a result of observational bias due to interstellar reddening and/or stellar evolution. Both LBVs/BHGs/WN9-11h stars and YHGs are present in small numbers- as anticipated due to the apparently short durations of these phases – in clusters spanning a comparatively wide range of ages (∼2–12 Myr). This appears to support the predictions of e.g. Groh et al. (2013) that both high and low mass stars pass through such evolutionary phases (the former always remaining in the blue region of the HR diagram and the latter on the bluewards track of a red loop).

Only two instances of clusters hosting confirmed sgB[e] stars are found – Wd1 and the Cyg OB2 association (MWC349A). Two further stars are of interest. Firstly Martayan et al. (2008) identify one member of NGC 6611 – the emission line binary W503 – as demonstrating an IR excess, which the authors attribute to the presence of a mass-transfer accretion disc. Further observations of this object to better constrain its nature would be of considerable value. Secondly, a detatched equatorial ring is associated with the ∼4 Myr old B1.5 Ia star Sher25, located in the outskirts of the young (∼1 Myr) cluster NGC 3603 (Brandner et al. 1997). Although the current stellar spectrum lacks the forbidden lines characteristic of sgB[e] stars (Smartt et al. 2002), Smith et al. (2007) suggest that Sher 25 might represent the evolved descendant of such a star.

Finally we strongly caution against employing these data in order to quantitatively determine the progenitor masses of evolved stars. In several cases the ages of clusters have been determined solely from the presence of particular spectral types; therefore deriving progenitor masses for such stars from the age of the cluster introduces a circularity into the argument. Moreover in many of the remaining cases ages have been inferred from isochrone fitting to sparse datasets, while in the near-IR window favoured for the study of obscured clusters isochrones are essentially vertical, presenting an additional difficulty. Finally, it is increasingly clear that binarity plays a major role in post-MS evolution (e.g. Clark et al. 2011); given that systematic RV surveys have only been attempted for a handful of clusters any detailed analysis of the data presented here would appear premature.

[11] Given the time that has elapsed, the properties of many of the clusters studied by these authors have been revised. This is apparent for e.g. Eggenberger et al. (2002), where new determinations of cluster ages have placed a number of clusters outside our 20 Myr cut-off (cf. NGC 3766, NGC 3590, NGC 5281, NGC 6664 and Trumpler 18), while a combination of (i) revisions in the classification of individual stars and (ii) the inclusion of stars of spectral-type A in their blue supergiant category explain both the discrepancies in number counts of red and bue supergiants between the works and the omission of additional clusters from our census (e.g. NGC 2384, NGC 6530, Trumpler 37 and Collinder 121, all of which now appear not to host supergiants).

[12] M17, W3, W31, W42, W51, G333.1-0.4, NGC 3576, Sh2-152, S255, and RCW34.

Table A.1. Stellar content of Galactic young massive clusters.

Cluster/ Complex	Age (Myr)	Mass ($10^3 M_\odot$)	B[e]	O2-6Ia(+)/ WN6-9ha	O7-9 I/ B0-9 I	LBV/BHG/ WN9-11h	YHG	RSG	WN	WC/ WO	Reference
Pismis 24	<1–2	–	0	1	0	0	0	0	0	1	1
NGC 3603	1–2	10–16	0	5	2	0	0	0	0	0	2, 3, 4
IC 1805	1–3	–	0	1	1	0	0	0	0	0	5, 6
Westerlund 2	<2.5	3	0	3	0	0	0	0	0	0	7, 8
NGC 6611	2–3	–	0	0	2	0	0	0	0	0	9, 10
Arches	2–4	>10	0	28	0	0	0	0	0	0	11
Mercer 23	2–4	3–5	0	3	5	0	0	0	0	0	12
Havlen-Moffat 1	2–4	–	0	5	0	0	0	0	0	0	1
DBS2003 179	2–5	>7	0	8	0	1	0	0	0	0	13, 14
NGC 6823	2–7	–	0	0	5	0	0	0	0	0	5
Ruprecht 44	2.1–3.5	–	0	0	0	0	0	0	1	0	1
Berkeley 86	2.5–3.4	–	0	0	0	0	0	0	1	0	1
Cl1806-20	3–4	>3	0	0	4	1	0	0	1	1	15
Glimpse 30	3–4.5	3	0	0	0	1	0	0	3	0	16
VVV CL011	3–7	1	0	1	0	0	0	0	0	0	17
Quartet	3–8	1.3–5.2	0	0	0	2	0	0	0	1	18
Berkeley 87	~3.2	–	0	0	2	1?	0	0	0	1	1
Quintuplet	3.3–3.6	>10	0	1	?	8	0	0	2	13	19, 20, 21
Pismis 20	3.6–6.0	–	0	0	1	0	0	0	1	0	1
Mercer 81	$3.7^{+0.4}_{-0.5}$	10	0	9	0	0	1	0	0	0	22, 23
Cl1813-178	4–4.5	10	0	2	12	1	0	1	3	0	24
Bochum 7	4.3 ± 0.5	–	0	0	0	0	0	0	1	0	25, 26
VVV CL009	4–6	1	0	1	5	0	0	0	0	0	17
VVV CL074	4–6	>2.5	0	1	0	0	0	1	1	1	17
VVV CL099	4–6	>1.6	0	0	0	0	0	0	1	1	17
NGC 6913	4–6	–	0	0	3	0	0	0	0	0	5, 27
Westerlund 1	~5	~100	1	0	>100	7	6	4	14	8	25, 28, 29
NGC 6604	5 ± 2	–	0	0	2	0	0	0	0	0	30, 31
VVV CL036	5–7	2.2	0	0	1	0	0	1	1	0	17
DBS2003 45	5–8	>2	0	0	6	0	0	0	0	0	32
Gal. Centre	6	>10	0	0	27	8	0	0	9	14	33, 34
NGC 6910	6 ± 2	–	0	0	1	0	0	0	0	0	35
Glimpse 20	6–8	3.4	0	0	1	0	1	0	0	1	18
NGC 7235	6–11	–	0	0	1	0	0	1	0	0	3, 36
VVV CL073	<7	>1.4	0	1	0	0	0	0	1	0	17
Markarian 50	~7.4	–	0	0	1	0	0	0	1	0	1
NGC 3293	8 ± 1	–	0	0	2	0	0	1	0	0	37, 38
NGC 2414	9	–	0	0	1	0	0	0	0	0	39, 40
IC 2581	10	–	0	0	1	0	0	0	0	0	41
Ruprecht 55	10	–	0	0	1	0	0	0	0	0	39, 42
NGC 654	>10	–	0	0	1	0	0	0	0	0	6, 43
NGC 4755	11	–	0	0	3	0	0	0	0	0	37, 44

Notes. Breakdown of the stellar content of known Galactic young stellar aggregates (≤20 Myr; clusters and OB associations) ordered approximately by increasing age. Clusters/associations hosting sgB[e] stars given in bold. The upper pannel consists of clusters, the lower of OB associations (broken down where possible into constituent clusters), non-coeval aggregates (ages given in itallics) and the cluster W43, for which no age is given (but its youth is indicated by its associated GH II region). NGC 3603 appears co-eval with the exception of the two BSGs Sher 23 and 25 which are suggestive of an older (~4 Myr) population. Regarding the GC cluster proper for simplicity we adopt the numbers of stars within the 2 coherent disc-like structures (Paumard et al. 2006) noting that a number of additional WR candidates (but no B[e] stars) have been identified in the surrounds. Classification of the Quintuplet OB supergiants is particularly difficult; via comparison to the Arches we reclassify LH099 as WN7-9ha but of the 84 stars Liermann et al. (2009) list as O stars we are unable to determine accurate spectral types and/or luminosity classes. Following the literature convention we restrict YHGs to spectral types A, F and G. Finally, we assign a tentative classification of LBV to V439 Cyg; a star with an uncertain history which Polcaro & Norci (1998) quote as being identified as respectively "Mira-like", B3e, a carbon star, B0ep, B1.5 Ve and a candidate LBV over the last ~70 yrs.

References. [1]Massey et al. (2001); [2]Harayama et al. (2008); [3]Melena et al. (2008); [4]Schnurr et al. (2008); [5]Massey et al. (1995); [6]Shi & Hu (1999); [7,8]Rauw et al. (2007, 2012); [9]Hillenbrand et al. (1993); [10]Martayan et al. (2008); [11]Martins et al. (2008); [12]Hanson et l. (2010); [13,14]Borissova et al. (2008, 2012); [15]Bibby et al. (2008); [16]Kurtev et al. (2007); [17]Chené et al. (2013); [18]Messineo et al. (2009); [19]Figer et al. (1999); [20,21]Liermann et al. (2009, 2012); [22]Davies et al. (2012b); [23]de La Fuente et al. (2013); [24]Messineo et al. (2011); [25]Crowther et al. (2006b); [26]Michalska et al. (2013); [27]Wang & Hu (2000); [28]Clark et al. (2005); [29] Negueruela et al. (2010a); [30]Barbon et al. (2000); [31]De Becker et al. (2005); [32]Zhu et al. (2009); [33]Paumard et al. (2006); [34]Martins et al. (2007); [35]Kolaczkowski et al. (2004); [36]Sowell (1987); [37]Evans et al. (2005); [38]Baume et al. (2003); [39]Kharchenko et al. (2005); [40]Fitzgerald et al. (1979); [41]Turner (1973); [42]Bosch et al. (2003); [43]Pandey et al. (2005); [44]Aidelman et al. (2012); [45,46]Davies et al. (2008, 2009); [47]Slesnick et al. (2002); [48]Currie et al. (2010); [49]Marco & Negueruela (2013); [50]Messineo et al. (2010); [51]Clark et al. (2009); [52]Negueruela et al. (2010b); [53]Negueruela et al. (2011); [54]González-Fernández & Negueruela (2012); [55]Davies et al. (2007a); [56]Zhang et al. (2012); [57]Fitzsimmons et al. (1993); [58]Ramsay & Pollacco (1992); [59]Kaltcheva et al. (2001); [60]Hanson (2003); [61]Negueruela et al. (2008); [62]Davies et al. (2012a); [63]Sana et al. (2006); [64]Ankay et al. (2001); [65]Smith (2006); [66]Blum et al. (1999).

Table A.1. continued.

Cluster/ Complex	Age (Myr)	Mass ($10^3 M_\odot$)	B[e]	O2-6Ia(+)/ WN6-9ha	O7-9 I/ B0-9 I	LBV/BHG/ WN9-11h	YHG	RSG	WN	WC/ WO	Reference
RSGC 1	12 ± 2	30 ± 10	0	0	0	0	1	14	0	0	45
Cl1900+14	13–15	1	0	0	4	0	0	2	0	0	46
$h + \chi$ Per	14	20	0	0	15	0	0	6	0	0	47, 48
NGC 7419	14 ± 2	7–10	0	0	0	0	0	5	0	0	49
Mercer 9	15–27	1.6 ± 0.4	0	0	2	0	0	3	0	0	50
RSGC 3	16–20	30 ± 10	0	0	0	0	0	16	0	0	51, 52
RSGC 4	16–20	>10	0	0	0	0	0	9	0	0	52
RSGC 5	16–20	>10	0	0	0	0	0	9	0	0	53
RSGC 6	16–20	>10	0	0	0	0	0	8	0	0	54
RSGC 2	17 ± 3	40 ± 10	0	0	0	0	0	26	0	0	55
NGC 457	20	–	0	0	0	0	0	1	0	0	56, 57
NGC 2439	20	–	0	0	1	0	0	1	0	0	58, 59
Cyg OB2	2–7	>10	1	6	11	2	0	0	2	3	60, 61
Danks 1+	$1.5^{+1.5}_{-0.5}$	8 ± 1.5	0	5	1	0	0	0	0	0	62
Danks 2+	3^{+3}_{-1}	3 ± 0.8	0	0	1	0	0	0	0	1	62
G305 field	–	–	0	1	0	0	0	0	3	4	62
NGC 6231+	*2.5–5*	–	0	0	2	0	0	0	0	1	63
Sco OB1	*2.5–5*	–	0	1	8	0	0	0	0	0	64
Trumpler 14 +	1.5	–	0	1	0	0	0	0	0	0	1, 65
Trumpler 16 +	2–3	–	0	4	3	0	0	0	0	0	1, 65
Collinder 228 + Trumpler 15 +	6 ± 3	–	0	0	1	0	0	0	0	0	1, 65
Bochum 10 +	7	–	0	0	1	0	0	0	0	1	1, 65
W 43	–	–	0	3	0	0	0	0	0	0	66
NGC 6871	*2–4*	–	0	0	2	0	0	0	1	0	1
Trumpler 27	*3–5*	–	0	0	7	0	0	1	0	2	1, 25
Total			**2**	**91**	**>251**	**31(+1?)**	**9**	**110**	**47**	**54**	